

1-14-2019

# Late Pleistocene Glaciation in the Mosquito Range, Colorado, U.S.A.: Chronology and Climate

Keith A. Brugger

*University of Minnesota, Morris*, [bruggeka@morris.umn.edu](mailto:bruggeka@morris.umn.edu)

Benjamin J.C. Laabs

*North Dakota State University--Fargo*

Alexander Reimers

*North Dakota State University--Fargo*

Noah Bensen

*University of Minnesota, Morris*, [bense034@morris.umn.edu](mailto:bense034@morris.umn.edu)

Follow this and additional works at: [https://digitalcommons.morris.umn.edu/geol\\_facpubs](https://digitalcommons.morris.umn.edu/geol_facpubs)

 Part of the [Glaciology Commons](#)

---

## Recommended Citation

Brugger, Keith A.; Laabs, Benjamin J.C.; Reimers, Alexander; and Bensen, Noah, "Late Pleistocene Glaciation in the Mosquito Range, Colorado, U.S.A.: Chronology and Climate" (2019). *Geology Publications*. 15.

[https://digitalcommons.morris.umn.edu/geol\\_facpubs/15](https://digitalcommons.morris.umn.edu/geol_facpubs/15)

This Article is brought to you for free and open access by the Faculty and Staff Scholarship at University of Minnesota Morris Digital Well. It has been accepted for inclusion in Geology Publications by an authorized administrator of University of Minnesota Morris Digital Well. For more information, please contact [skulann@morris.umn.edu](mailto:skulann@morris.umn.edu).

1 **Late Pleistocene Glaciation in the Mosquito Range, Colorado, U.S.A.: Chronology and Climate**

2 Keith A. Brugger<sup>1</sup>, Benjamin Laabs<sup>2</sup>, Alexander Reimers<sup>2</sup>, Noah Bensen<sup>3</sup>

3 <sup>1</sup>Geology Discipline, University of Minnesota, Morris, Morris, MN, U.S.A. 56267

4 <sup>2</sup>Department of Geosciences, North Dakota State University, Fargo, ND, U.S.A 58102

5 <sup>3</sup>Chemistry Discipline, University of Minnesota, Morris, Morris, MN, U.S.A. 56267

6 **Abstract**

7 New cosmogenic <sup>10</sup>Be surface exposure ages from seventeen moraine boulders in the Mosquito Range  
8 suggest that glaciers were at their late Pleistocene (Pinedale) maximum extent at ~21–20 ka, and that ice  
9 recession commenced prior to ~17 ka. These age limits suggest that the Pinedale Glaciation was  
10 synchronous within the Colorado Rocky Mountain region. Locally, the previous (Bull Lake) glaciation  
11 appears to have occurred no later than 117 ka, possibly ~130 ka allowing for reasonable rock weathering  
12 rates. Temperature-index modeling is used to determine the magnitude of temperature depression required  
13 to maintain steady-state mass balances of seven reconstructed glaciers at their maximum extent.  
14 Assuming no significant differences in precipitation compared to modern values, mean annual  
15 temperatures were ~8.1 and 7.5 °C cooler, respectively, on the eastern and western slopes of the range  
16 with quantifiable uncertainties of +0.8/–0.9 °C. If an average temperature depression of 7.8 °C is assumed  
17 for the entire range, precipitation differences - that today are 15-30% greater on the eastern slope due to  
18 the influence of winter/early spring snowfall - might have been enhanced. The temperature depressions  
19 inferred here are consistent with similarly derived values elsewhere in the Colorado Rockies and those  
20 inferred from regional-scale climate modeling.

21 **Keywords:** Colorado; Pinedale glaciation; cosmogenic exposure dating; glacial chronology; paleoclimate

22 **Introduction**

23 The precise timing of Late Pleistocene glacial advances and deglaciation in the western United States and  
24 the magnitude of their respective causative forcings inform our understanding of paleoclimate dynamics  
25 (Licciardi *et al.*, 2004; Thackray, 2008). Despite the increasing number of well-constrained glacial  
26 chronologies across the montane western U.S. (e.g. Phillips *et al.*, 1990, 1996, 2009; Gosse *et al.*, 1995;  
27 Licciardi *et al.*, 2001, 2004; Leonard *et al.*, 2017a; Licciardi and Pierce, 2018), additional studies are  
28 needed in order to better define spatial and temporal patterns of glacier behavior and climate during the  
29 last Pleistocene glaciation. Specifically, asynchronous glacier behavior might reveal the influence of  
30 secondary climatic factors or internal dynamics affecting response that are superimposed on global-scale  
31 drivers of climate change (e.g insolation and atmospheric CO<sub>2</sub>). These include differences in glacier  
32 hypsometry, local or microclimate (i.e. sub-regional energy and mass balances), and/or glacier response

33 times (e.g. Thackray, 2008; Laabs *et al.*, 2009; Young *et al.*, 2011). Glacial chronologies also provide a  
34 temporal context for proxies of Late Pleistocene climate inferred from glacier fluctuations. Because the  
35 Last Glacial Maximum (LGM), in particular, represents a unique climatic state very different than those  
36 of the subsequent 20 ka, glacial records provide important information unavailable from many other  
37 sedimentary and biological records (e.g. pollen spectra) because of limits of the length of the respective  
38 records or geographic coverage. Thus glacial chronologies and their value for understanding LGM  
39 climate represent fundamental data that are critical in evaluating the skill of models (so-called  
40 “hindcasting”) used to project future global change (Braconnot *et al.*, 2012; Flato *et al.*, 2013; Kageyama  
41 *et al.*, 2017). The increasing number of precise glacial chronologies notwithstanding, few (e.g. Ward *et al.*  
42 *et al.*, 2009; Leonard *et al.*, 2017a) have been integrated with modeling approaches to infer details  
43 concerning climate change during the last glaciation.

44 Addressing the need for both additional glacial chronologies and climate reconstructions in the Rocky  
45 Mountains, we present here new cosmogenic  $^{10}\text{Be}$  surface-exposure ages of moraines and model-derived  
46 limits on Late Pleistocene climate from the Mosquito Range, Colorado, an area that has received little  
47 attention with respect to its glacial history. Exposure ages obtained from moraine boulders indicate  
48 glaciers achieved their last Pleistocene maximum extent ca. 21–20 ka and overall deglaciation  
49 commenced by 17 ka. Our results suggest the timing of moraine occupation in the Mosquito Range agrees  
50 with recent Pleistocene glacial chronologies developed in adjacent ranges in Colorado. Limits on the last  
51 glacial climate in the study area are inferred from temperature-index modeling, which determines  
52 temperature depressions required to maintain steady-state mass-balances of reconstructed paleoglaciers.  
53 Our estimates of temperature depression in the Mosquito Range are in excellent agreement with those  
54 similarly determined in the region.

## 55 **Study Area**

56 The Mosquito Range is a north-south trending range bordered by the upper Arkansas River valley and  
57 Sawatch Range to the west and South Park and the southern Front Range to the east (Fig. 1). The  
58 Arkansas River valley is a topographic expression of the northernmost extent of the Rio Grande Rift that  
59 became tectonically active ca. 30–25 Ma (Kellogg *et al.*, 2017). Many peaks exceed 4000 m and features  
60 typical of alpine glaciation and periglacial activity characterize landscapes at higher elevations.  
61 Structurally the range is cored by Precambrian crystalline rocks unconformably overlain by complexly  
62 faulted and folded Paleozoic clastics and carbonates that were later intruded by a suite of Tertiary sills,  
63 dikes, and small plutons (McCalpin *et al.*, 2012a, b; Kellogg *et al.*, 2017).

64 Late-Quaternary glaciation in the Mosquito Range was characterized by extensive valley glacier  
65 systems (Fig. 2a). These systems were to a large degree interconnected either by virtue of common ice  
66 fields and/or pervasive ice divides. The ice fields also solely supported several small ice lobes. In some  
67 locations glaciers in adjacent valleys coalesced to form composite termini. Glaciers were more extensive  
68 in the northern part of the range where ice masses were contiguous with ice sourced from the Tenmile  
69 Range and other isolated peaks. An east-west asymmetry with respect to glacier length and area existed  
70 during the LGM that becomes more pronounced in the central and southern part of the range. Glaciers had  
71 both greater lengths and surface areas on the eastern slope. Although the elevations of catchment areas are  
72 comparable (~3600–3800 m), glaciers there terminated at lower elevations than did those on the western  
73 slopes. Well-preserved terminal and lateral moraines of the last (Pinedale) and penultimate (Bull Lake)  
74 glaciations are common at the mouths of glaciated valleys, and in most are delineated on bedrock maps  
75 (Widmann *et al.*, 2007; McCalpin *et al.*, 2012a, b; Bohannon and Ruleman, 2013; Kellogg *et al.*, 2017).  
76 The relative ages of these moraines can generally be distinguished by morphostratigraphic criteria (e.g.  
77 boulder abundance and freshness, sharpness of moraine crests, etc.). In these valleys recessional moraines  
78 of the Pinedale Glaciation are also evident.

79 Modern climate in the Mosquito Range is continental, with mean annual temperatures (MAT) of ~2  
80 °C at the mountain fronts (~3000 m) and ~-5 °C at the highest elevations (>4000 m). (Data from the  
81 stations shown in Fig. 1 are derived available through the Western Regional Climate Center,  
82 <http://wrcc.dri.edu>, and the National Water and Climate Center, <http://wcc.nrcs.usda.gov>, in addition to  
83 that provided by the PRISM Climate Group, Oregon State University, <http://prism.oregonstate.edu>.)  
84 Mean January and July temperatures typically deviate from the mean annual temperature by  $\pm 10$  °C  
85 irrespective of elevation. For a given elevation, MATs tend to be on average ~1 °C warmer on the eastern  
86 slope of the range at elevations between 3000 and 3700 m. At the highest elevations (>3700), MAT are  
87 slightly cooler by ~ 0.5 °C.

88 Mean annual precipitation (MAP) varies from ~40 cm at the lowest elevation of the range to ~120 cm  
89 on the high peaks, averaging ~76 cm. The monthly/seasonal distribution of precipitation varies over the  
90 range; however, the general pattern is bimodal with an early maximum in late winter/early spring and a  
91 later maximum corresponding to mid-to-late summer (Fig. 3a). The earlier maximum is more muted at the  
92 lowest elevations but at higher elevations it is comparable to or greater than the later maximum.

93 For much of the year, moist Pacific air is delivered to the Colorado Rocky Mountains by prevailing  
94 westerly flow. The Mosquito Range, being essentially on the eastern boundary, therefore receives less  
95 precipitation than ranges farther west. However, during the late winter and early spring, synoptic  
96 circulation patterns cause upslope precipitation of southeasterly Gulf of Mexico-derived moisture. This

97 disproportionately affects the eastern slopes. Mid- to late summer precipitation is associated with the North  
98 American monsoon (Higgins *et al.*, 1997) that brings moisture from the Gulfs of both Mexico and  
99 California. The PRISM model yields an area-averaged value for MAP for the eastern slope of ~0.8 m  
100 while that for the western slope is ~0.7 m. Given similar elevations, available station records also suggest  
101 the eastern slope receives ~0.1 m more precipitation annually than does the western slope. More  
102 significantly for this study, winter precipitation (October-April) at elevations between 3000 and 3500 m  
103 (Fig. 3b) is ~13% greater on the eastern slope. Disregarding the Fremont Pass SNOTEL site that appears  
104 to be anomalous, this disparity increases to ~20%. Extrapolation of the respective trends suggests that at  
105 higher elevations (3500–4200 m) the eastern slope could receive as much as 30% more precipitation  
106 during the winter.

## 107 **Methods**

### 108 *Cosmogenic <sup>10</sup>Be exposure dating*

109 Ten boulders from mapped terminal moraine complexes of the Pinedale glaciation in three glaciated  
110 valleys were sampled for exposure ages, specifically in the valleys of Iowa Gulch, Twelvemile Creek, and  
111 Fourmile Creek (Fig 4). In Big Union Creek, four boulders were sampled from a moraine that was/is  
112 interpreted as being deposited during a recessional stillstand or minor readvance of ice after the terminal  
113 moraine was abandoned. Sampling of the terminal moraine in this valley, about one kilometer  
114 downvalley, was avoided because of its poor preservation and lack of suitable boulders. Similarly, the  
115 *only* boulder suitable and/or accessible for sampling in the Sacramento valley was on the distal slope of a  
116 recessional moraine (Fig. 4). Additionally, two boulders on a moraine segment mapped as pre-Pinedale in  
117 the Iowa Gulch valley (Kellogg *et al.*, 2017) were sampled. Boulders selected for sampling were located  
118 on or as close to moraine crests as possible, and all were granitic lithologies. Where possible, samples  
119 were collected from the tops of boulders standing >1 m over the moraine surface, however boulders  
120 having heights as little as ~0.4 m were also sampled. Preference was given to boulders exhibiting smooth,  
121 polished surfaces but given the coarse nature of the lithologies some sampled boulders did not meet this  
122 criterion. Large boulders suitable for sampling on several other moraine segments preserved in the study  
123 area were extremely scarce. The reason for this scarcity is unclear, but agreement among exposure ages  
124 for each sampled moraine crest suggests that boulder removal or degradation by weathering and erosion  
125 has been minimal. Moreover, some moraines in the study area were on private property and were  
126 therefore not accessible for sampling. Altogether, seventeen samples were ultimately prepared for  
127 cosmogenic isotope analyses and submitted for <sup>10</sup>Be/<sup>9</sup>Be measurement by accelerator mass spectrometry;  
128 see Supporting Information for details concerning sample information, processing, and calculation of <sup>10</sup>Be  
129 exposure ages.

130 *Glacier reconstruction*

131 Field mapping of glacial features to verify and augment those shown on existing geologic maps,  
 132 examination of topographic maps and digital elevation models, and use of Google Earth® imagery  
 133 allowed for the determination of the maximum extents of seven paleoglaciers (Fig. 2) on the basis of  
 134 lateral-terminal moraine complexes and the upper limits of glacial erosion. Ice surface contours were  
 135 reconstructed by considering mapped ice limits, flow patterns delineated by large-scale erosional forms  
 136 (e.g. valley trends, streamlined bedrock, roche moutonnées), and general convergent and divergent flow  
 137 in the accumulation and ablations area respectively. Contours were adjusted iteratively so that  
 138 reconstructed ice surface slopes were sub-parallel to those of the valley and to ensure driving stresses  $\tau$   
 139 were between 50 and 150 kPa commonly measured on modern glaciers (Cuffey and Paterson 2010).  
 140 Stresses were calculated using:

$$141 \quad \tau = S_f \rho g h \sin \alpha \quad (1)$$

142 where  $\rho$  is the density of ice,  $g$  is gravitational acceleration,  $h$  is ice thickness,  $\alpha$  is the slope of the ice  
 143 surface, and  $S_f$  is a shape factor to account for drag of the valley sides (Nye, 1965). The surface slope was  
 144 averaged over distances of  $10h$  to account for longitudinal stress gradients (Bindschadler *et al.*, 1977;  
 145 Cuffey and Paterson, 2010).

146 *Temperature-index modeling*

147 The temperature-index model (TM) used here is a modified version of what was presented in Brugger  
 148 (2010). In short, the TM is used to find the temperature and precipitation changes required to maintain  
 149 steady-state mass-balances of the reconstructed glaciers. To this end an approach was sought that  
 150 minimized tuning of model parameters.

151 The variation of the *annual* specific mass-balance (i.e., at a point)  $b_n$  with elevation  $z$  is simulated by:

$$152 \quad b_n(z) = \int_{t_1}^{t_2} (P_s(t, z) + M(t, z)) dt \quad (2)$$

153 where  $P_s(t, z)$  is the rate of snow accumulation,  $M(t, z)$  the rate of snow or ice melt (ablation) over the  
 154 glacier's surface during the interval  $t_1$  to  $t_2$  (the hydrologic year). In practice Equation (2) is numerically  
 155 integrated over a monthly time-scale to yield monthly melt that is then combined with available monthly  
 156 precipitation data and then integrated over the hydrologic year.

157 Melt is determined using a melt (or degree-day) factor  $m_f$  that empirically relates ablation to mean  
 158 daily air temperature  $T_d(t, z)$ :

$$159 \quad M(z, t) = \begin{cases} m_f T_d(t, z) & T_d(t, z) > T_m \\ 0 & T_d(t, z) \leq T_m \end{cases} \quad (3)$$

160 where  $T_m$  is a threshold temperature above which melting occurs.

161 The simplicity of the empirical approach to ice and snow ablation implicit in Equation (3) has the  
 162 advantage of requiring far less meteorological data and/or parameterization than “enhanced” temperature-  
 163 index models, or other energy balance approaches, wherein a radiation balance is considered.  
 164 Furthermore, temperature-index methods perform well over basin-size spatial scales and intervals of time  
 165 exceeding a few days (Hock, 1999; 2003). In recent comparisons of approaches to *long-term* ablation  
 166 simulation, the performance of simple temperature-index methods compared favorably to, and in some  
 167 instances exceeded, more physically-based models (e.g. Vincent and Six, 2013; Réveillet *et al.*, 2017) or  
 168 otherwise point to shortcomings of energy-balance models (Gabbi *et al.*, 2014). Thus TMs are especially  
 169 suitable for determination of temperature depression during glaciation given the suite of meteorological  
 170 and atmospheric unknowns.

171 Simulations were run using  $T_m = +1$  °C but also 0 °C given both values have been used in previous  
 172 studies (e.g. Hock, 1999; Pellicciotti *et al.* 2005; Gabbi *et al.*, 2014; Réveillet *et al.*, 2017;). Values  $m_f$  for  
 173 snow and ice are taken as 0.45 and 0.80 cm water equivalent (w.e.)  $d^{-1} °C^{-1}$ , respectively as these are  
 174 reasonable means of  $m_f$  values obtained for relatively debris-free ice and snow on modern glaciers (Hock,  
 175 2003; Braithwaite, 2008; Brugger, 2010). However, although there are outliers,  $m_f$  values for snow  
 176 reported in the literature typically range from  $\sim 0.3$  to  $\sim 0.6$  cm w.e.  $d^{-1} °C^{-1}$ , while those for ice lie between  
 177  $\sim 0.6$  and 1.0 cm w.e.  $d^{-1} °C^{-1}$ . Thus we show subsequently that our results are not unduly sensitive to the  
 178 precise values of  $m_f$ . The latter is also significant in light of research that indicates degree-day factors  
 179 vary spatially owing to local energy balances, for example topographic shading or surface slope and  
 180 aspect, and temporally according to climate and weather (Hock, 2003; Pellicciotti *et al.*, 2005; Mathews *et*  
 181 *al.*, 2015). In the TM the value of  $m_f$  is initially set for that of snow, but once snow melt exceeds  
 182 accumulation it changes to that for ice.

183 In contrast to previous applications of the TM (Brugger, 2006; 2010) in which air temperature was  
 184 assumed to vary sinusoidally about some annual mean, the algorithm used here is:

$$185 \quad T_a(z, t) = \left[ H \left[ \frac{1 - \cos\left(\frac{2\pi d}{365} - \phi\right)}{2} \right]^k - T_{jan}(z) \right] - \Delta T \quad (4)$$

186 where  $H$  is the magnitude of the yearly temperature variation,  $d$  is the day of the year,  $\phi$  is the phase lag  
 187 ( $= 0.359$  rads), and  $T_{jan}(z)$  is the mean January temperature at elevation  $z$ , and  $\Delta T$  is a prescribed  
 188 perturbation of mean annual temperature (i.e. LGM temperature depression). Values of  $T_{jan}(z)$  are  
 189 calculated using modern lapse rates obtained using available data (Table 1) with respect to  $T_{jan}(z)$  at a  
 190 reference elevation. Table 1 also shows that a significant difference in the January lapse rate exists

191 between the eastern and western sides of the Mosquito Range (also for other months) reflecting the  
 192 difference in climates (which are also represented in the monthly PRISM models). Note that  
 193 implementation of Equation (4) implies a uniform perturbation of temperature over the year, that is no  
 194 temperature seasonality is examined in the present study. The constant  $k$  in Equation (4) is a tuning  
 195 parameter that controls the sharpness of the temperature curve and allowed a better fit to observed  
 196 temperatures. Values of  $k$  (1.46 on the east side of the range, 1.45 on the west) were chosen to minimize  
 197 the root mean square error  $RMSE$  between simulated mean monthly temperatures and those recorded at all  
 198 relevant meteorological stations. Particular attention was on accurately simulating temperatures during the  
 199 ablation season (discussed subsequently). Values of  $H$  are remarkable consistent at all elevations on each  
 200 side of the range (Table 1).

201 Snow accumulation  $P_s(t,z)$  is determined by:

$$202 \quad P_s(t,z) = fP_{mod}(t,z) + F \quad (5)$$

203 where  $P_{mod}(t,z)$  is the modern precipitation,  $f$  is a partitioning function that determines what fraction of  
 204 monthly precipitation fall as snow based on a continuous function of air temperature (Brugger, 2010), and  
 205  $F$  is a prescribed change in precipitation (i.e. assumed changes in precipitation during glaciation). Values  
 206 for  $P_{mod}(t,z)$  are calculated from the monthly fraction of the respective seasonal (winter, spring, summer,  
 207 fall) totals and corresponding vertical precipitation gradients (Table 1). This approach is also a departure  
 208 from previous implementations of the TM that used a vertical precipitation gradient based solely on mean  
 209 annual precipitation. Use of seasonal gradients ensured that simulated precipitation, particularly that  
 210 during the accumulation season (i.e. late fall to early spring), was not unduly influenced by the “steep”  
 211 summer gradients that are significantly different and are poorly defined. It should be noted that summer,  
 212 and more generally all, rain — not treated in temperature-index methods — can contribute to ablation but  
 213 its contribution is usually negligible for non-maritime glaciers (Cuffey and Paterson, 2010). Monthly  
 214 precipitation gradients for each season do not significantly differ (<10%) justifying the use of seasonal  
 215 averages. The monthly fraction of seasonal precipitation is largely independent over the elevation range  
 216 of interest here (~3000–4000m) with values varying less than ~10% during the accumulation season.

## 217 **Results**

### 218 *Cosmogenic $^{10}\text{Be}$ exposure ages*

219 Cosmogenic  $^{10}\text{Be}$  exposure ages at Iowa Gulch (Table 3) yield distinct populations of ages across the two  
 220 sampled moraine crests (Fig. 4). Two, zero-erosion exposure ages on the outer moraine are  $115 \pm 6$  ka  
 221 and  $120 \pm 5$  ka, corresponding to the last global interglaciation during MIS 5e (Lisiecki and Raymo,  
 222 2005). The assumption of zero erosion at the boulder surface is inconsistent, however, with studies of  
 223 exposed coarse-grained granitic rocks elsewhere in the Rocky Mountains (Benedict, 1993; Small *et al.*,



224 1997). Although it is not possible to precisely limit the rate of boulder surface erosion, Benedict (1993)  
225 estimated a time-averaged erosion rate of  $1 \text{ mm kyr}^{-1}$  at a similar altitude and latitude in Colorado.  
226 Applying that same erosion rate to surfaces IG-01-16 and IG-02-16 yields exposure ages of  $133 \pm 3 \text{ ka}$   
227 and  $127 \pm 4 \text{ ka}$ . These ages align with the end of MIS 6, the time of the penultimate global glaciation.  
228 Cosmogenic  $^{10}\text{Be}$  exposure ages of four boulders atop the inner moraine in Iowa Gulch yield a mean  
229 exposure age of  $20.6 \pm 1.1 \text{ ka}$  ( $1\sigma$ ). Three of the four exposure ages overlap at  $1\sigma$ , with the fourth  
230 exposure (sample IG-04-16) being somewhat younger than the oldest three. We conclude that the mean of  
231 all four exposure ages represents the true age of the moraine, which is firmly within MIS 2.

232 In Union Canyon, four exposure ages (Table 3) from atop the recessional moraine ( $\sim 1 \text{ km}$  upvalley  
233 from the outermost Pinedale moraine; Fig. 4) feature three overlapping exposure ages with a mean of  $17.1$   
234  $\pm 0.4 \text{ ka}$  and one older exposure age (of  $20.1 \pm 0.5 \text{ ka}$ ) that does not overlap with the younger three at  $2\sigma$ .  
235 The older exposure age is more consistent with the age of the terminal Pinedale moraine in Iowa Gulch,  
236 suggesting that ice in both valleys was at or near the maximum extent at  $\sim 20 \text{ ka}$ . The younger three  
237 exposure ages in Union Canyon indicate that the ice was also near its maximum extent at  $17.1 \pm 0.4 \text{ ka}$ .

238 Cosmogenic  $^{10}\text{Be}$  exposure ages of Pinedale-age terminal and recessional moraines in the valleys of  
239 Twelvemile, Fourmile, and Sacramento Creeks (Table 3) are consistent with those at Iowa Gulch and  
240 Union Canyon, with a single exposure age from the terminal Pinedale moraine at Twelvemile Creek of  
241  $20.6 \pm 0.5 \text{ ka}$  and two exposure ages at Fourmile Creek with a mean of  $21.7 \pm 1.6 \text{ ka}$ . One significantly  
242 older exposure age of the Fourmile Creek terminal moraine of  $61.3 \pm 0.6 \text{ ka}$  and a slightly older age of  
243  $28.6 \pm 1.0 \text{ ka}$  on the Twelvemile Creek terminal moraine are interpreted as older outliers, possibly  
244 reworked boulders with  $^{10}\text{Be}$  inventory from a period of prior exposure. A single younger exposure age  
245 from a recessional moraine in Fourmile Creek valley of  $13.3 \pm 0.2 \text{ ka}$  is difficult to interpret without  
246 additional data, but may represent a late ice advance in the valley. The age of the only sample taken in the  
247 Sacramento Creek valley,  $17.4 \pm 1.3 \text{ ka}$ , is consistent with those from the recessional moraine in Union  
248 Canyon.

#### 249 *Glacier Reconstructions*

250 The geometries of the reconstructed glaciers (Fig. 2) are summarized in Table 2. Driving stresses tend to  
251 be low ( $\sim 50 \text{ kPa}$ ) in the lower reaches of the reconstructed glaciers (Fig 2b). While not unreasonable,  
252 these most likely represent minimum values given underestimates of ice thickness due to post-LGM  
253 glacial and fluvial valley fill. Extrapolation of the bedrock walls of valley profiles suggests thicknesses  
254 (and therefore driving stresses) could have been as much 10-20% greater than estimated here.  
255 Additionally, in several valleys terminal moraine complexes are characterized by an abundance of ice  
256 disintegration/stagnation features that might also point to low driving stresses. Stresses of  $\sim 70$  to  $150 \text{ kPa}$

257 are inferred for mid- and upper reaches of the reconstructed glaciers, the larger values being associated  
258 with steep surface slopes, associated with those of the underlying bedrock, and/or greater ice thickness.

259 Reconstructions indicate that glacier extent was greatest in the northern Mosquito Range, as noted  
260 previously, and that glaciers were larger on the eastern slope. A full explanation of this east-west  
261 asymmetry is beyond the scope of this work, but could certainly involve the land surface topography and  
262 possible precipitation differences during the last glaciation. An analysis of the hypsometry shows that the  
263 total land area above 3500 m, essentially corresponding to a rough average of equilibrium-line altitudes  
264 (ELAs, discussed subsequently), is almost 40% larger on the eastern side of the range (261 km<sup>2</sup> versus  
265 191 km<sup>2</sup>). While this analysis does not take into consideration slope angles, it nevertheless suggests a  
266 greater extent of areas of potential accumulation for glaciers on the east. Combined with the possibility of  
267 greater precipitation, total accumulation may have been significantly greater as well.

#### 268 *Temperature-index modeling: model verification*

269 The robustness of the TM was evaluated by its ability to simulate modern climate and modern snowpack  
270 evolution at specific localities. It should be emphasized that local temperature and precipitation values are  
271 not explicitly used in the model, but rather determined from regional parameters. Figures 5a and b show  
272 that over the elevations most relevant to paleoglacier extents (~3000-4200 m), simulated temperatures  
273 agree quite well with those observed. Simulated temperatures during the ablation season are most critical  
274 because they drive melting. Temperatures during most of the accumulation season are less critical as these  
275 are well below the threshold for melting. Agreement during the ablation season is quantified by  $RMSE_{abl}$   
276 values that are less than 1 °C. Cumulative temperature differences over the ablation season  $\Sigma\Delta_{abl}$  are also  
277 low, being less than  $\pm 0.5$  °C. (Note that positive and negative values indicate the model respectively  
278 overestimates or underestimates a given quantity.) These values are representative of all other stations.

279 Similarly, the accuracy of modeled precipitation is more important during the accumulation season.  
280 Figures 5c and d (again typical of all stations in the appropriate elevation range) show that the model  
281 provides accurate representations of modern precipitation. Modeled values show less agreement with  
282 observations at Fremont Pass, however this station is somewhat outside the immediate study area.  
283 Climax, located two kilometers closer lies at essentially the same elevation yet receives ~8 cm (12%) less  
284 precipitation annually. Such spatial variability in precipitation is not uncommon (Anderton *et al.*, 2004)  
285 and has been noted elsewhere in the region (Brugger, 2010). The Fremont Pass station notwithstanding,  
286 errors over the accumulation season ( $RMSE_{acc}$ ) are < 1 cm for all stations between 3000 and 3500 m.  
287 Modeled precipitation on the east side of the Mosquito Range for the four stations of interest yield  
288 cumulative differences ( $\Sigma\Delta_{acc}$ ) in precipitation of  $\sim \pm 2.5$  cm for the accumulation season (Fig. 5d) On the  
289 western slope,  $\Sigma\Delta_{acc}$  is between  $\pm 4.0$  cm (three stations; data from the Leadville stations were averaged).

290 Perhaps the most stringent criteria to test the TM is how well it simulates modern snow accumulation  
 291 and snowpack evolution (in w.e.) recorded in SNOTEL records (Figs. 5e and f) because this is most  
 292 closely related to the goal of simulating glacier mass-balance. Simulations of the three SNOTEL records  
 293 on the eastern side of the range are quite good with due consideration of, among others: (1) temporal  
 294 differences in resolution (daily versus monthly in the model); (2) possible wind drifting or deflation of  
 295 snow at observations sites (Meyer *et al.*, 2012); (3) the effects of a tree canopy on local accumulation and  
 296 ablation (Varhola *et al.*, 2010). These factors can result in measured snow water equivalents at SNOTEL  
 297 sites that are not representative of their surroundings (Molotch and Bales, 2005). Nevertheless, RMSE  
 298 values (October-June/July) are less than 4.5 cm w.e. Because these reflect in part differences in temporal  
 299 resolution, the differences ( $\Delta_{snow}$ ) in the maximum snow water equivalent might provide another metric of  
 300 the ability of the TM to simulate snow accumulation.  $\Delta_{snow}$  values ranged from  $-1.6$  cm w.e. at the Rough  
 301 and Tumble site to  $+4.1$  cm w.e. at the Buckskin site (Fig 5f). Similar comparisons on the western slope  
 302 of the Mosquito Range are problematic. Figure 5e shows that the model simulates less well the record at  
 303 the Fremont Pass site (RMSE = 8.9 cm w.e.,  $\Delta_{snow} = -9.7$  cm w.e.), the only SNOTEL on the west side of  
 304 the range. However, this is an artifact of the inability of the model (and the inherent precipitation  
 305 gradients used) to accurately simulate modern precipitation at this location as noted previously.  
 306 Therefore, a “synthetic” record of snow accumulation at the Climax site was created by using cumulative  
 307 (monthly) snow depths there and determining the mean density for late fall through early spring snowfall  
 308 using data available for Fremont Pass. Agreement between the model and the synthetic record is better  
 309 (RMSE = 3.0 cm w.e.,  $\Delta_{snow} = +7.9$  cm w.e.), especially allowing for uncertainties in assumed snow  
 310 density (Fig. 5e).

311 Varying  $m_f$  by  $\pm 0.2$  cm w.e.  $d^{-1} \text{ } ^\circ\text{C}^{-1}$  results in a change in maximum snowpack(s) by no more than  
 312  $\pm 3\%$ . The only significant impact of this variation is to alter the length of time snow persists into the  
 313 spring/summer (see for example the Hoosier Pass record in Fig. 6f). Changing the threshold temperature  
 314 for melt ( $T_m$  in Equation (3)) to  $0^\circ\text{C}$  reduces maximum snowpack(s) by only a maximum of  $\sim 3\%$  at all  
 315 sites.

### 316 *Temperature-index modeling: inferring Late Pleistocene glacial climate*

317 Climate during the last glaciation is determined by finding the temperatures and/or precipitation that  
 318 satisfy:

$$319 \quad B_n = \int_A b_n dA \approx \sum_{i=1}^j b_{n_i} A_i = 0 \quad (6)$$

320 where  $B_n$  is the steady-state mass-balance,  $A$  is glacier area composed of  $j$  number of discrete elevation  
 321 intervals, and  $b_{n_i}$  is the mean annual specific net-balance over  $A_i$ . We emphasize that Equation (6)  
 322 explicitly considers glacier hypsometry. However, solving Equation (6) presents the problem of

323 equifinality, that is there are an infinite number of solutions that satisfy the condition  $B_n = 0$ . Therefore,  
324 reasonable limits must be imposed on assumed temperature-precipitation combinations.

325 With regard to the foregoing, the most straightforward assumption is that precipitation during the last  
326 glaciation was comparable to that today (i.e.  $F = 0$  (Equation (5))). Under this assumption, simulations  
327 suggest temperature depressions between 7.9 and 8.2 °C are required to maintain steady-state mass  
328 balances of glaciers on the east side and between 7.4 and 7.7 °C on the west side of the Mosquito Range  
329 (Table 4). The respective averages are  $8.1 \pm 0.3$  °C and  $7.5 \pm 0.2$  °C. Uncertainties for individual  
330 estimates of temperature depression were +0.8 and -0.9 °C based on sensitivity analysis of the TI model  
331 (see Supporting Information for a complete analysis).

332 The associated ELAs are consistently lower on the east than on the west side of the range, averaging  
333  $\sim 3485 \pm 30$  m and  $3575 \pm 25$  m respectively. Average ELAs determined using the accumulation-area ratio  
334 method (AAR = 0.65) are lower than their simulated counterparts by  $\sim 10$  to 45 m but show a similar  
335 consistency (Table 4). Lower ELAs on the east side of the range might also suggest that differences  
336 between precipitation on the eastern and western slopes of the Mosquito Range similar to those today  
337 existed during the last glaciation. This is discussed further in a subsequent section.

338 Whether precipitation during the last glaciation differed from that of today is more challenging to  
339 assess because the Colorado Rocky Mountain region lacks paleoclimate proxies that might constrain  
340 precipitation. Moreover, despite their resolution, global and regional climate simulations of the last  
341 glaciation from model ensembles suggest only slight changes in precipitation in this region and are  
342 equivocal whether climate was wetter or drier (e.g. Braconnot *et al.* 2007; Oster *et al.*, 2015; Lora *et al.*,  
343 2017). Differences in precipitation are also indicated by climate reconstructions using pollen-based  
344 proxies (Izumi and Bartlein, 2016). Thus it is prudent to consider scenarios in which the last glaciation in  
345 the Mosquito Range was wetter or drier.

346 Figure 6 shows the effect of potential changes in precipitation on the temperature depression required  
347 for steady-state glacier mass-balances. Not surprisingly, greater/smaller temperature depression (i.e.  
348 less/more ablation) must be offset by concomitant reductions/increase in precipitation (less  
349 accumulation). Given the magnitudes suggested by paleoclimate reconstructions for western North  
350 America (Kim *et al.*, 2008; Ibarra *et al.*, 2014; Oster *et al.*, 2015; Lora *et al.*, 2017), we allow annual  
351 precipitation to vary slightly by  $\pm 10$  cm. Changes of this magnitude are  $\pm 15$ -25% of modern MAP values  
352 (depending on location and elevation) and therefore might be considered too great. Table 4 and Figure 6  
353 show that under slightly wetter conditions the required temperature depressions are  $7.5 \pm 0.3$  °C for the  
354 eastern side and  $7.0 \pm 0.2$  °C for the western side of the range. If the last glacial climate was slightly drier,  
355 the corresponding temperature depressions are  $8.9 \pm 0.3$  and  $8.0 \pm 0.2$  °C respectively. Assuming

356 arguably extreme changes in precipitation, say +50 cm and –20 cm — not supported by any studies of  
357 which we are aware — the required temperature depressions might have been between ~5.6 and 9.9 °C  
358 (Fig. 6). (Note that reductions in precipitation by more than 20 cm are precluded as this results in no  
359 precipitation at lower elevations.)

## 360 Discussion

### 361 *Chronology of glacial deposits*

362 On the Bull Lake moraine segment in Iowa Gulch, the mean of two  $^{10}\text{Be}$  ages is  $130 \pm 5$  ka after  
363 allowing for a reasonable rate of rock erosion ( $1 \text{ mm kyr}^{-1}$ ). Schweinsberg *et al.* (2017), using the same  
364 erosion rate and a similar cosmogenic-isotope production scaling model, obtained a mean age of  $132 \pm 8$   
365 ka for four boulders on a Bull Lake-aged moraine fronting the Lake Creek Valley on the eastern side of  
366 the Sawatch Range (TL on Fig. 1b). Unfortunately, there are few other exposure ages for comparably-  
367 aged moraines elsewhere in Colorado. Benson *et al.* (2004) found anomalously young  $^{36}\text{Cl}$  ages on four of  
368 five Bull Lake boulders in the Park and Front Ranges that were attributed to combination of erosion,  
369 snow and sediment shielding, and  $^{36}\text{Cl}$  leakage. The fifth yielded a zero-erosion, shielding uncorrected  
370 age of ~144 ka (original value). Dethier *et al.* (2000) reported *minimum* mean  $^{10}\text{Be}$  and  $^{26}\text{Al}$  ages of  $101 \pm$   
371  $21$  ka and  $122 \pm 26$  ka (original values) on Bull Lake moraines in the Front Range. Schildgen *et al.* (2002)  
372 dated an associated Bull Lake terrace at  $133 \pm 28$   $^{10}\text{Be}$  ka and  $139 \pm 31$   $^{26}\text{Al}$  ka (original values). The  
373 younger minimum ages notwithstanding, these age estimates are in good agreement and indicate broad  
374 regional synchrony of glacial advances during MIS 6.

375 Exposure ages obtained on Pinedale-age (MIS 2) terminal moraines in the Mosquito Range (Table 3)  
376 span an interval from  $22.8 \pm 0.2$  to  $19.0 \pm 0.6$  ka. Five overlapping ages (Fig. 7a) yield a mean age of  $20.9$   
377  $\pm 0.4$  ka. Alternatively, inclusion of the oldest and youngest ages yields an identical mean age of  $20.9 \pm$   
378  $1.1$  ka. The probability density plot shows a dominant peak at 20.6 ka. Several authors (e.g. Applegate *et*  
379 *al.*, 2010; Heyman *et al.*, 2011; Leonard *et al.*, 2017b) have pointed out that the ages (mean, distribution,  
380 and so forth) of moraine boulders can be interpreted differently. We follow Leonard *et al.* (2017b) and  
381 numerous other studies by using the mean exposure age to indicate the timing of moraine abandonment  
382 following the maximum ice extent, while at the same time providing a minimum age for the Pinedale  
383 maximum. Thus we argue that the last glaciation in the Mosquito Range culminated at ~20–21 ka during  
384 the latter part of the global Last Glacial Maximum (26.5 to 19.0 ka; Clark *et al.*, 2009). This timing is  
385 consistent with the conclusions of a recent review of available cosmogenic exposure ages in Colorado by  
386 Leonard *et al.* (2017b) wherein they showed that individual valley glacier maxima generally occurred  
387 prior to ~19.5 ka.

388 Leonard *et al.* (2017b) also concluded that retreat or abandonment of terminal moraines in Colorado  
389 was asynchronous, possibly well underway at ~17–16 ka in the San Juan Mountains and Front Range,  
390 while glaciers remained at or near their maximum extents in the Sawatch Range and Sangre de Cristo  
391 Mountains at that time. The younger <sup>10</sup>Be ages on the recessional moraine in Union Canyon (Fig. 4)  
392 suggest that, at least in this valley, glaciers were close to their maximum extent at ~17 ka suggesting a  
393 similar early deglaciation history in the Mosquito Range as those in the immediately adjacent ranges. This  
394 apparent asynchronous response across the region begs the question as to what climatic conditions and/or  
395 dynamic factors allowed glaciers to persist at or nearly maximum extents in some glacial valleys and not  
396 others. Asynchronous glacier maxima in the Sawatch Range was reported by Young *et al.* (2011), who  
397 suggest that differences in glacier shape, aspect, and hypsometry may have resulted in temporal  
398 differences in valley glacier advance and retreat during the last glaciation. It is worth noting, however,  
399 that more extensive ice in the Sawatch Range, the Sangre de Cristo Mountains and Mosquito Range at  
400 ~17 ka is coeval with glacier maxima and/or readvances documented in other glaciated ranges in the U.S.  
401 Rocky Mountains as further discussed below.

#### 402 *Glacial chronology and regional climate*

403 The Pinedale maximum in the Mosquito Range at 21–20 ka was coincident with an insolation  
404 minimum (Fig. 7g) and cooler Northern Hemispheric temperatures (Fig. 7b). It corresponded to the global  
405 LGM (Clark *et al.*, 2009; Lisiecki and Raymo, 2005), the time when southern outlets of the Laurentide  
406 Ice Sheet were at their maximum extent (Ullman *et al.*, 2015), and with mountain glacier maxima  
407 elsewhere in the Rocky Mountains of Utah (Laabs *et al.*, 2009; Quirk *et al.*, 2018) and Wyoming (Dahms  
408 *et al.*, 2018). This time interval also featured wetter and/or cooler winters reflected in speleothem records  
409 from the southwestern U.S. (Fig. 7d-f). Paleohydrologic studies (Ibarra *et al.*, 2014; 2018) indicate  
410 minimal increases in LGM precipitation in the northern Great Basin (at latitudes greater than the  
411 Mosquito Range) but much greater increases at latitude similar to the Mosquito Range, suggesting the  
412 latter proxies may reflect precipitation increases during the Pinedale Maximum.

413 Extensive ice at 17 ka is coeval with glacier maxima in the nearby Sangre de Cristo Range (Leonard  
414 *et al.*, 2017a) and Sawatch Range (Young *et al.*, 2011; Schweinsberg *et al.*, 2016) and with glacier  
415 readvances to near maximum lengths in the Wasatch and Uinta Ranges of the Middle Rocky Mountains  
416 (Laabs and Munroe, 2016; Quirk *et al.*, 2018), and maximum extents of several outlet glaciers of the  
417 Greater Yellowstone Glacial System (Licciardi and Pierce, 2008, 2018; their “middle Pinedale). The  
418 potential driver of glacier readvance or persistence near their maximum lengths may be related to regional  
419 precipitation changes following the LGM (e.g., Thackray *et al.*, 2004; Thackray, 2008). This is consistent  
420 with the observed highstands of many of the pluvial lakes in the Southwestern U.S. at 17-16 ka (Fig. 7c;  
421 Munroe and Laabs, 2013), coeval wetter and/or cooler conditions as revealed by speleothem records (Fig.

422 7d-f; Wagner *et al.*, 2010; Asmerom *et al.*, 2010; Moseley *et al.*, 2016) and reconstructed lake highstands  
423 (Lyle *et al.*, 2012; Ibarra *et al.*, 2014; 2018) following the initial phase of deglaciation. The timing of  
424 these events falls within the Heinrich Stadial 1 (ca. 18-15 ka; Figs. 7 and 8) that is associated with a  
425 hemispheric cooling owing to a weakening of the Atlantic Meridional Overturning Circulation (McManus  
426 *et al.*, 2004). However, regional asynchrony of deglaciation and in the highstands of some pluvial lakes  
427 (Munroe and Laabs, 2013; Ibarra *et al.*, 2014) implies a degree of local modulation of hemispheric  
428 climate forcing(s).

#### 429 *Last glacial climate in the Mosquito Range*

430 Our results suggest that in the absence of any changes in precipitation, temperatures in the Mosquito  
431 Range were between 7.5 and 8.1 °C cooler during the Pinedale maximum compared to modern.  
432 Considering the uncertainty (+0.8/-0.9°C), these values agree and one could conclude there was no  
433 significant difference in temperature depression with respect to the eastern and western slopes. In detail,  
434 however, the difference is largely an artifact of those in modern, and presumed last glacial precipitation.  
435 This begs the question as to whether temperature depression could have differed over the range. A  
436 reasonable assumption is that regional temperature was more uniform than precipitation. If an average  
437 glacial temperature depression of 7.8 °C for the whole of the Mosquito Range is assumed, a precipitation  
438 increase of ~5 cm over modern is required on the eastern side of the range while a decrease of similar  
439 magnitude is required on the western side (Fig. 6). This outcome therefore suggests that the difference in  
440 precipitation across the range observed today was somewhat accentuated during the last glaciation.

441 Independent estimates of ELAs based on the AAR method (Table 4) that are consistently lower on the  
442 eastern side of the range compared to the western side might also point to differences in precipitation.  
443 Refsnider *et al.* (2009) noted a similar cross-range difference in ELAs in the Sangre de Cristo Mountains  
444 ~100 km to the south. They attributed this to an enhancement of late winter/early spring southeasterly-  
445 derived (Gulf of Mexico) moisture that would have preferentially nourished glaciers on the eastern slopes.  
446 We offer this as a viable explanation for the *apparent* east-west differences in Late Pleistocene glacial  
447 temperature depression obtained by our simulations. This conclusion is consistent with the fact that  
448 modern winter precipitation – presumably therefore snow accumulation – is greater on the eastern slopes  
449 of the Mosquito Range due to late winter/early spring events.

450 Interestingly, a high-resolution paleoclimate simulation for North America (Kim *et al.*, 2008; their  
451 Fig. 8) indicates a sharp east-west gradient in LGM winter precipitation (December-February in their  
452 study) in the general region of the study area. Their simulation suggests that this gradient arises by a  
453 combination of increases over modern precipitation in the east and decreases in the west, and by  
454 magnitudes greater than those implied by our simulations. Thus our conclusion that the present difference

455 in winter precipitation across the Mosquito Range not only existed during the last glaciation, but was  
456 could have been more pronounced, is not unreasonable. Moreover, *if* the North American summer  
457 monsoon strengthened (*cf.* Lachniet *et al.*, 2013; Bhattachary *et al.*, 2017), then greater increases in  
458 precipitation on the eastern slopes that would fall as snow at higher elevations, would have further  
459 increased accumulation differences across the range.

460 Our average estimate of glacial temperature depression of  $7.8 +0.8/-0.9$  °C in the Mosquito Range  
461 compares favorably with estimates elsewhere in the Colorado Rocky Mountains (Table 5). (Unless,  
462 otherwise indicated, subsequent comparisons assume no significant changes in precipitation.) Brugger  
463 (2010), using a slight variation of the TM used in the present study, found MATs were on average  $6.9 \pm$   
464  $0.6$  °C cooler for the southern Sawatch Range and Elk Mountains to the west. In the same area, Brugger  
465 and Goldstein (1999) suggested a temperature depression of  $7.0-9.0$  °C based on climatic interpretation  
466 of lowered ELAs. Preliminary TM simulations (Brugger *et al.*, 2017) suggests a LGM temperature  
467 depression of  $\sim 6.2$  and  $\sim 7.5$  °C to maintain glaciers in the northern Sawatch Range, immediately to the  
468 west of the study area. Refsnider *et al.* (2009) concluded that mean summer temperatures in the Sangre de  
469 Cristo Mountains in southern Colorado were  $\sim 6.0-7.5$  °C cooler, varying according to assumed changes  
470 in precipitation. In a sub-region of those same mountains, the Blanca Massif, Brugger *et al.* (2009)  
471 suggested  $7.0-8.0$  °C of cooling based on TM simulations. In contrast, Leonard *et al.*, (2017a) using a  
472 coupled energy-mass balance-flow model, determined that LGM temperatures were  $\sim 5.0 +1.5/-1.0$  °C  
473 cooler in the Sangre de Cristo Mountains. Leonard and Russell (in Schweinsberg, *et al.*, 2016) applied the  
474 same approach and determined temperatures were depressed  $5.4$  °C in the northern Sawatch. Dühnforth  
475 and Anderson (2011), who employed a numerical model of glacier flow with parameterized mass-balance  
476 components, found that temperatures were between  $4.5$  and  $5.8$  °C cooler in Front Range, farther afield to  
477 the northeast. In a broader regional study based on climate at equilibrium-lines, Leonard (1989)  
478 concluded temperatures in Colorado were  $\sim 8.5$  °C cooler. Leonard (2007) later used this approach within  
479 a GIS-based model and concluded that Late Pleistocene glaciers in central Colorado would have required  
480 an average temperature depression of  $7.6 \pm 0.7$  °C.

481 The relatively small disparities in estimates of last glacial temperature depression are undoubtedly  
482 due in part to differences in the methodologies used, and they are perhaps smaller than they first appear  
483 when considering the associated uncertainties (when reported). There are, however, other potential  
484 explanations that might either wholly or partially reconcile these differences. First, LGM temperature  
485 depression during the Pinedale maximum might have indeed vary throughout the region; that is, an *a*  
486 *priori* assumption that regional temperature (and precipitation) change during the Pinedale was uniform  
487 and not modulated by local, or microclimatic influences is questionable. Climate simulations of the LGM  
488 indicate changes in MATs in the specific geographic areas referenced above were between  $\sim -8.0$  and –



489 10.0 °C (e.g. Paleoclimate Modeling Intercomparison Project 3 ensemble means, Oster *et al.*, 2015,  
490 Supplementary Table S-9; Community Climate System Model (CCSM) 3, Lorenz *et al.*, 2016; CCSM4,  
491 data available at WorldClim - Global Climate Data, <http://www.worldclim.org>). While these results  
492 appear to corroborate the idea that temperature change during the Pinedale maximum might have varied  
493 somewhat, the stated  $1\sigma \sim \pm 2.9$  °C associated with these means precludes any definite conclusion.

494 The foregoing methodologies also depend on the extents of paleoglaciers delineated by terminal  
495 moraines and their precise relationship with regional climate. Additional complications in directly  
496 comparing derived temperature depression can be therefore introduced by virtue of potential ambiguities  
497 in the relationships among/between climate forcing(s), glacier response, and interpretations of moraine  
498 ages (Kirkbride and Winkler, 2012). A full discussion of these is beyond the scope of this study, rather  
499 they are outlined here in order to provide a context for comparing the timing and magnitude of glacial  
500 cooling in the Colorado Rocky Mountains. In short, the Pinedale maximum (used here in the strict sense  
501 of the timing of maximum downvalley glacier extent) might have been time-transgressive (Young *et al.*,  
502 2011) and spatially variable owing to (1) microclimates modulating regional/global climate differently so  
503 local forcings were asynchronous; (2) differences in valley glacier response times (e.g. Pelto and  
504 Hedlund, 2001; Brugger, 2007a) related to glacier hypsometries, (Young *et al.*, 2011; Chenet *et al.*, 2010)  
505 or valley topography (Pratt-Sitaula *et al.*, 2011) that led to asynchronous behavior; and/or (3) maximum  
506 glacier extent is not indicative of the mean glacial climate but rather a reflection of a single, transient  
507 response(s) to stochastic interannual variations in temperature (Anderson *et al.*, 2014). Therefore,  
508 attaching inordinate significance to *minor* differences in estimates of LGM temperature depression should  
509 perhaps be avoided.

## 510 **Conclusions**

511 Moraine boulder <sup>10</sup>Be surface exposure ages in four valleys in the Mosquito Range reveal that terminal  
512 moraine deposition occurred during MIS 6 and MIS 2. During the Pinedale Glaciation, valley glaciers  
513 were at or near their maximum extents ~21–20 ka. Exposure ages of boulders on a recessional moraine  
514 suggest that ice retreat was under way by ~17 ka. Temperature-index modeling suggests that during the  
515 Pinedale maximum, steady-state mass balances of glaciers on the east side of the range required  
516 temperatures that were on average 8.1 °C less than modern, assuming no change(s) in precipitation.  
517 Glaciers on the west side of the range existed under temperatures 7.5 °C cooler. Given uncertainties of  
518 +0.8/–0.9 °C, a glacial temperature depression of 7.8 °C is implied. Under the assumption that  
519 temperature depression was uniform over the Mosquito Range, precipitation differences that exist today  
520 across the range might have been enhanced during the last glaciation, potentially by strengthening of the

521 North American summer monsoon. If precipitation increased or decrease slightly ( $\pm 10$  cm) as suggested  
522 by some climate reconstructions, temperature depression could have been between 7.0 and 8.9 °C.

523 Within the bounds of uncertainties, the new chronology for the last glaciation in the Mosquito Range  
524 presented here is in good agreement with those developed for the northern Sawatch Range and Elk  
525 Mountains, the Front Range, the Sangre de Cristo Mountains, and the San Juan Mountains. The timing of  
526 the LGM in the Colorado Rocky Mountains thus appears to have been broadly synchronous and driven by  
527 regional cooling and perhaps slight enhancements in winter precipitation. In contrast, initial deglaciation  
528 was asynchronous, beginning first in the Front Range and San Juan Mountains and later in the Mosquito  
529 Range, Sawatch Range, and Sangre de Cristo Mountains.

530 Our estimate(s) of temperature change in the Mosquito Range during the Pinedale maximum is also  
531 consistent with those similarly-derived for other mountain ranges in Colorado and with those based on  
532 climate at ELAs. Furthermore, it is consistent with temperature depressions inferred from regional-scale  
533 modeling of LGM paleoclimate. Differences exist, however, between our estimate and those based on  
534 coupled glacier flow-mass-balance models that yield temperature depressions on the order of 5–6 °C.  
535 These differences, while possibly real, are small considering the associated quantifiable uncertainties in  
536 the approaches used *combined with* the possibility of spatially varying changes in LGM precipitation.

### 537 **Supporting Information**

538 **Text.** Processing of moraine boulder samples and calculation of  $^{10}\text{Be}$  exposure ages, and modeling  
539 uncertainties.

540 **Table S1.** Cosmogenic  $^{10}\text{Be}$  sample data and exposure ages.

541 **Table S2.** Sensitivity analysis of the TI model and resulting uncertainties.

### 542 **Acknowledgements**

543 Funding for initial cosmogenic dating and fieldwork was provided to KAB by the UMM's Faculty  
544 Research Enhancement Funds. A seed grant to KAB and BL from the Purdue University PRIME Lab  
545 provided AMS analyses of additional samples. NB was supported by the University of Minnesota's  
546 Undergraduate Research Opportunity Program. BL and AR gratefully acknowledge support of the NDSU  
547 College of Science and Math. We also thank the reviewers for their thorough and thoughtful comments.

### 548 **References**

549 Asmerom, Y., Polyak, V.J., Burns, S.J., 2010. Variable winter moisture in the southwestern United States  
550 linked to rapid glacial climate shifts. *Nat. Geosci.* 3, 114e117.

- 551 Anderson LS, Roe GH, Anderson RS. 2014. The effects of interannual climate variability on the moraine  
552 record. *Geology* **42**: 55-58.
- 553 Anderton SP, White SM, Alvera B. 2004. Evaluation of spatial variability in snow water equivalent for a  
554 high mountain catchment. *Hydrologic Processes* **18**: 435–453.
- 555 Applegate PJ, Urban NM, Laabs BJC, *et al.* 2010. Modeling the statistical distributions of cosmogenic  
556 exposure dates from moraines. *Geoscientific Model Development* **3**: 293-307.
- 557 Benedict JB. 1993. Influence of snow upon rates of granodiorites weathering, Colorado Front Range  
558 USA. *Boreas* **22**: 87–92.
- 559 Benson L, Madole R, Phillips *et al.* 2004. The probable importance of snow and sediment shielding on  
560 cosmogenic ages of north-central Colorado Pinedale and pre-Pinedale moraines. *Quaternary Science*  
561 *Reviews* **23**: 193-206.
- 562 Berger, A. 1992. Orbital variations and insolation database. IGBP PAGES/World Data Center for  
563 Paleoclimatology, Data Contribution Series 92-007, NOAA/NGDC Paleoclimate Program, Boulder  
564 Colorado, USA.
- 565 Bhattacharya T, Tierney JE, DiNezio P. 2017. Glacial reduction of the North American Monsoon via  
566 surface cooling and atmospheric ventilation. *Geophysical Research Letters* **44**: 5113–5122.
- 567 Bindschadler R, Harrison WD, Raymond CF *et al.* 1977. Geometry and dynamics of a surge-type  
568 glacier. *Journal of Glaciology* **18**: 181-194.
- 569 Bohannon RG, Ruleman CA. 2013. Geologic map of the Mount Sherman 7.5' Quadrangle, Lake and Park  
570 Counties, Colorado. United States Geologic Survey Scientific Investigation Map 3271.
- 571 Braconnot P, Otto-Bliesner B, Harrison S *et al.* 2007. Results of PMIP2 coupled simulations of the Mid-  
572 Holocene and Last Glacial Maximum – Part 1: experiments and large-scale features. *Climates of the*  
573 *Past* **3**: 261-277.
- 574 Braconnot P, Harrison SP, Kageyama M *et al.* 2012. Evaluation of climate models using paleoclimatic  
575 data. *Nature Climate Change* **2**: 417-424.
- 576 Braithwaite, RJ. 2008. Temperature and precipitation climate at the equilibrium-line altitude of glaciers  
577 expressed by the degree-day factor for melting snow. *Journal of Glaciology* **54**: 437-444.
- 578 Brugger KA. 2006. Late Pleistocene climate inferred from the reconstruction of the Taylor River Glacier  
579 Complex, southern Sawatch Range, Colorado. *Geomorphology* **75**: 318-329.
- 580 Brugger KA. 2007a. The non-synchronous response of Rabots Glaciär and Storglaciären to recent climate  
581 change: a comparative study. *Annals of Glaciology* **46**: 275-282.
- 582 Brugger KA. 2010. Climate in the southern Sawatch Range and Elk Mountains, Colorado, USA, during  
583 the Last Glacial Maximum: inferences using a simple degree-day model. *Arctic, Antarctic, and Alpine*  
584 *Research* **42**: 164-178.
- 585 Brugger KA, Goldstein BS. 1999. Paleoglacier reconstruction and late-Pleistocene equilibrium-line  
586 altitudes, southern Sawatch Range, Colorado. In *Glacial Processes Past and Present*, Mickelson DM,  
587 Attig JW (eds.), Geological Society of America Special Paper 337; 103–112.
- 588 Brugger KA., Refsnider KA, Leonard, EM. 2009. Late Pleistocene climate on the Blanca Massif, Sangre  
589 de Cristo Range, Colorado. *Geological Society of America Abstracts with Programs* **41**: 640.
- 590 Brugger KA, Ruleman CA, Caffee MW. 2017. Glaciation and climate during the Last Glacial Maximum  
591 in the Mount Massive region, northern Sawatch Range, Colorado. *Geological Society of America*  
592 *Abstracts with Programs* **49**: 6.
- 593 Chenet M, Roussel E, Jomelli V *et al.* 2010. Asynchronous Little Ice Age glacial maximum extent in  
594 southeast Iceland. *Geomorphology* **114**: 253-260.
- 595 Clark PU, Dyke AS, Shakun JD *et al.* 2009. The last glacial maximum. *Science* **325**: 710-714.
- 596 Cuffey KM, Paterson WSB. 2010. *The Physics of Glaciers (4th ed.)*. Elsevier, Boston.

- 597 Dahms D, Egli M, Fabel D *et al.* 2018. Revised Quaternary glacial succession and post-LGM recession,  
598 southern Wind River Range, Wyoming, USA. *Quaternary Science Reviews* **192**: 167-184.
- 599 Dethier DP, Schildgen TF, Bierman P *et al.* 2000. The cosmogenic isotope record of late Pleistocene  
600 incision, Boulder Canyon, Colorado. *Geological Society of America Abstracts with Programs* **32**:  
601 473.
- 602 Dühnforth M, Anderson RS. 2011. Reconstructing the glacial history of green lakes valley, North Boulder  
603 Creek, Colorado Front Range. *Arctic, Antarctic, and Alpine Research*. **43**: 527-542.
- 604 Flato G, Marotzke J, Abiodun B *et al.* 2013. Evaluation of climate models. In *Climate Change 2013: The*  
605 *Physical Science Basis. Contribution of Working Group I to the Fifth Assessment Report of the*  
606 *Intergovernmental Panel on Climate Change*. Stocker, TF, Qin D, Plattner GK, *et al.* (eds).  
607 Cambridge University Press, Cambridge and New York; 741-866.
- 608 Gabbi J, Carenzo M, Pellicciotto F *et al.* 2014. A comparison of empirical and physically based glacier  
609 surface melt models for long-term simulation of glacier response. *Journal of Glaciology* **60**: 1140-  
610 1154.
- 611 Gosse JC, Klein J, Lawn B *et al.*, 1995. Beryllium-10 dating of the duration and retreat of the last  
612 Pinedale glacial sequence. *Science* **268**: 1329-1333.
- 613 Higgins RW, Yao Y, Wang XL. 1997. Influence of the North American Monsoon system on the U.S.  
614 summer precipitation regime. *Journal of Climate* **10**: 2600-2622.
- 615 Hock R. 1999. A distributed temperature-index ice- and snowmelt model including potential direct solar  
616 radiation. *Journal of Glaciology* **45**: 101-111.
- 617 Hock R. 2003. Temperature index melt modelling in mountain areas. *Journal of Hydrology* **282**: 104-  
618 115.
- 619 Heyman J, Stroeve AP, Harbor JM *et al.* 2011. Too young or too old: evaluating cosmogenic exposure  
620 dating based in an analysis of compiled boulder ages. *Earth and Planetary Science Letters* **302**: 71-  
621 80.
- 622 Ibarra DE, Egger AE, Weaver KL, *et al.* 2014. Rise and fall of late Pleistocene pluvial lakes in response  
623 to reduced evaporation and precipitation: evidence from Lake Surprise, California. *Geological Society*  
624 *of American Bulletin* **126**: 1387-1415.
- 625 Ibarra DE, Oster JL, Winnick, MJ *et al.* 2018. Warm and cold wet states in the western United States  
626 during the Pliocene–Pleistocene. *Geology* **46**: 355-358.
- 627 Izumi K, Bartlein, PJ. 2016. North American paleoclimate reconstructions for the Last Glacial Maximum  
628 using an inverse modeling through iterative forward modeling approach applied to pollen data,  
629 *Geophysical Research Letters* **43**: 10,965–10,972.
- 630 Kageyama M, Albani S, Braconnot *et al.* 2017. The PMIP4 contribution to CMIP6 - Part 4: scientific  
631 objectives and experimental design of the PMIP4-CMIP6 last glacial maximum experiments and  
632 PMIP4 sensitivity experiments. *Geoscientific Model Development* **10**: 4035-4055.
- 633 Kellogg KS, Shroba RR, Ruleman CA *et al.* 2017. Geologic map of the Upper Arkansas River Valley  
634 region, north-central Colorado. United States Geologic Survey Scientific Investigation Map 3382.
- 635 Kim S-J, Crowley TJ, Erickson DJ, *et al.* 2008. High-resolution climate simulation of the last glacial  
636 maximum. *Climate Dynamics* **31**: 1-16.
- 637 Kirkbride MP, Winkler S. 2012. Correlation of Late Quaternary moraines: impact of climate variability,  
638 glacier response, and chronological resolution. *Quaternary Science Reviews* **46**: 1–29.
- 639 Laabs BJC, Munroe JS. 2016. Late Pleistocene mountain glaciation in the Lake Bonneville basin.  
640 In *Developments in Earth Surface Processes* **20**: 462-503.
- 641 Laabs BJ, Refsnider KA, Munroe JS *et al.* 2009. Latest Pleistocene glacial chronology of the Uinta  
642 Mountains: support for moisture-driven asynchrony of the last deglaciation. *Quaternary Science*  
643 *Reviews* **28**: 1171-1187.

- 644 Lachniet MS, Asmerom Y, Bernal JP *et al.* 2013. Orbital pacing and ocean circulation-induced collapses  
645 of the Mesoamerican monsoon over the past 22,000 y. *Proceedings of the National Academy of*  
646 *Sciences* **110**: 9255-9260.
- 647 Leonard EM. 1989. Climatic change in the Colorado Rocky Mountains: estimates based on modern  
648 climate at late Pleistocene equilibrium lines: *Arctic and Alpine Research* **21**: 245-255.
- 649 Leonard EM. 2007. Modeled patterns of Late Pleistocene glacier inception and growth in the Southern  
650 and Central Rocky Mountains, USA: sensitivity to climate change and paleoclimatic implications.  
651 *Quaternary Science Reviews* **26**: 2152-2166.
- 652 Leonard EM, Laabs BJC, Plummer MA *et al.* 2017a. Late Pleistocene glaciation and deglaciation in the  
653 Crestone Peaks area, Sangre de Cristo Mountains, USA - chronology and paleoclimate. *Quaternary*  
654 *Science Reviews* **158**: 127-144.
- 655 Leonard EM, Laabs BJC, Schweinsberg *et al.* 2017b. Deglaciation of the Colorado Rocky Mountains  
656 following the Last Glacial Maximum. *Cuadernos de Investigación Geográfica* **43**: 497-526.
- 657 Licciardi JM, Clark PU, Brook EJ *et al.* 2001. Cosmogenic <sup>3</sup>He and <sup>10</sup>Be chronologies of the late Pinedale  
658 northern Yellowstone ice cap, Montana, USA. *Geology* **29**: 1095-1098.
- 659 Licciardi JM, Clark PU, Brook EJ *et al.* 2004. Variable responses of western U.S. glaciers during the last  
660 deglaciation. *Geology* **32**: 81-84.
- 661 Licciardi JM, Pierce KL. 2008. Cosmogenic exposure-age chronologies of Pinedale and Bull Lake  
662 glaciations in greater Yellowstone and the Teton Range, USA. *Quaternary Science Reviews* **27**: 814-  
663 831.
- 664 Licciardi JM, Pierce KL. 2018. History and dynamics of the Greater Yellowstone Glacial System during  
665 the last two glaciations. *Quaternary Science Reviews* **200**: 1-33.
- 666 Lisiecki LE, Raymo ME. 2005. A Pliocene-Pleistocene stack of 57 globally distributed benthic  $\delta^{18}O$   
667 records. *Paleoceanography* **20**: PA1003.
- 668 Lora JM, Mitchell JL, Risi C *et al.* 2017. North Pacific atmospheric rivers and their influence on western  
669 North America at the Last Glacial Maximum. *Geophysical Research Letters* **44**, 1051-1059.
- 670 Lorenz DJ, Nieto-Lugilde D, Blois JL *et al.* 2016. Downscaled and debiased climate simulations for  
671 North America from 21,000 years ago to 2100 AD. *Scientific Data* **3**.
- 672 Lyle M, Heusser L, Ravelo C *et al.* 2012. Out of the Tropics: The Pacific, Great Basin Lakes, and the late  
673 Pleistocene water cycle in the western United States. *Science* **337**: 1629-1633.
- 674 Matthews T, Hodgkins R, Wilby RL *et al.* 2015. Conditioning temperature-index model parameters on  
675 synoptic weather types for glacier melt simulations. *Hydrologic Processes* **29**: 1027-1045.
- 676 McCalpin JP, Funk J, Mendel D. 2012. Leadville South Quadrangle Geologic Map, Lake County,  
677 Colorado. Colorado Geological Survey, Denver, Colorado.
- 678 McCalpin JP, Temple J, Sicard K *et al.* 2012. Climax Quadrangle Geologic Map, Lake and Park  
679 Counties, Colorado. Colorado Geological Survey, Denver, Colorado.
- 680 McManus JF, Francois R, Gherardi J-M *et al.* 2004. Collapse and rapid resumption of the Atlantic  
681 meridional circulation linked to deglacial climate changes. *Nature* **428**: 834-837.
- 682 Meyer JDD, Jin J, Wang S-Y. 2012. Systematic patterns of the inconsistency between snow water  
683 equivalent and accumulation precipitation as reported by the snowpack telemetry network. *Journal of*  
684 *Hydrometeorology* **13**: 1970-1976.
- 685 Molotch NP, Bales RC. 2005. Scaling snow observations from the point to the grid element: Implications  
686 for observation network design. *Water Resources Research* **41**: W11421
- 687 Moseley GE, Edwards RL, Wendt KA *et al.* 2016. Reconciliation of the Devils Hole climate record with  
688 orbital forcing. *Science* **351**: 165-168.
- 689 Munroe JS, Laabs BJC. 2013. Temporal correspondence between pluvial lake highstands in the  
690 southwestern US and Heinrich Event 1. *Journal of Quaternary Science* **28**: 49-58.

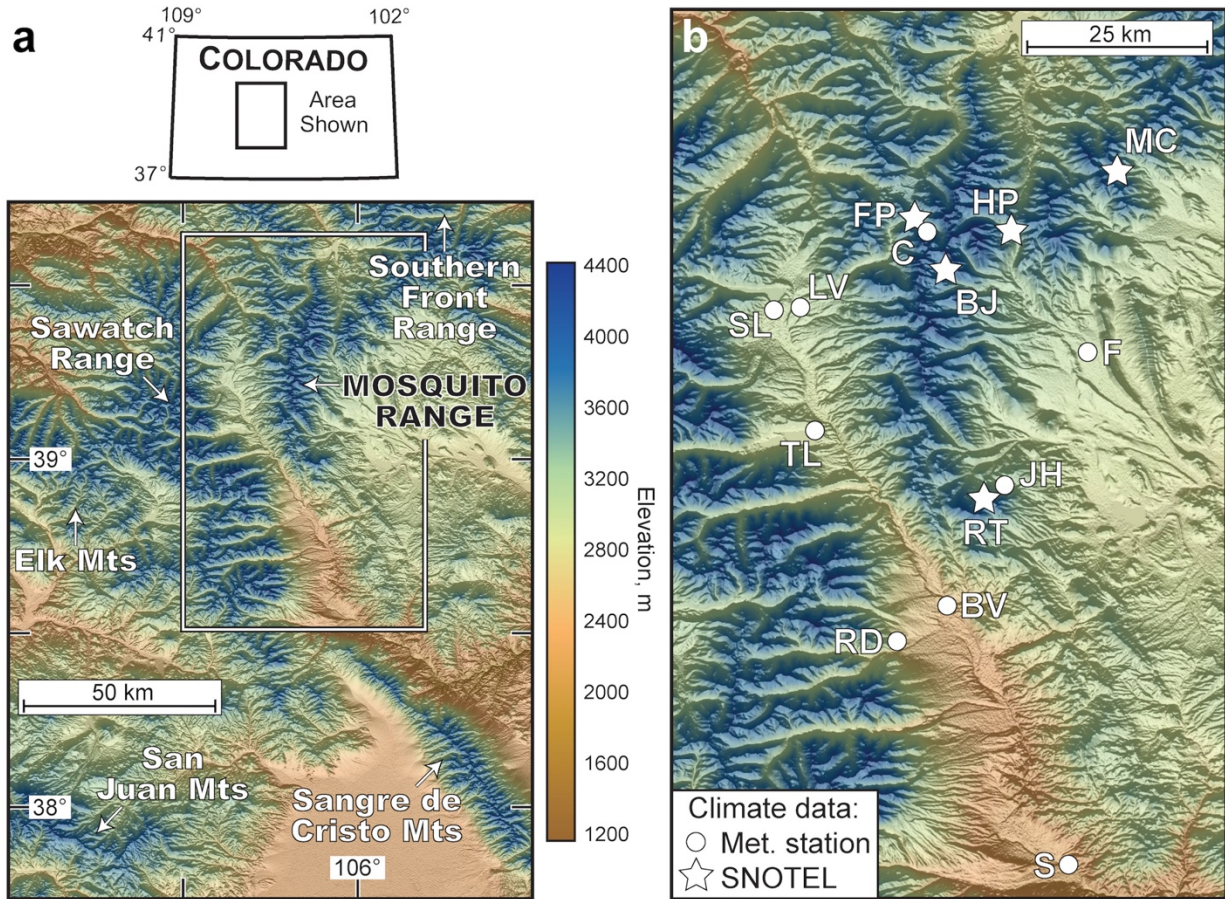
- 691 Nye JF. 1965. The flow of a glacier in a channel of rectangular, elliptic or parabolic cross-  
692 section. *Journal of Glaciology*, **5**: 661-690.
- 693 Oster JL, Ibarra DE, Winnick, MJ *et al.* 2015. Steering of westerly storms over western North America at  
694 the Last Glacial Maximum. *Nature Geoscience* **8**: 201-205.
- 695 Pellicciotti F, Brock B, Strasser U *et al.* 2005. An enhanced temperature-index glacier melt model  
696 including a shortwave radiation balance: development and testing for Haut Glacier d'Arolla,  
697 Switzerland. *Journal of Glaciology* **175**: 573-587.
- 698 Pelto MS, Hedlund C. 2001. Terminus behavior and response time of North Cascade glaciers,  
699 Washington, USA. *Journal of Glaciology*, **47**: 497-506.
- 700 Phillips FM, Zreda MG, Smith SS *et al.* 1990. Cosmogenic chlorine-36 chronology for glacial deposits at  
701 Bloody Canyon, eastern Sierra Nevada. *Science* **248**: 1529-1532.
- 702 Phillips FM, Zreda MG, Benson LV *et al.* 1996. Chronology of fluctuations in late Pleistocene Sierra  
703 Nevada glaciers and lakes. *Science* **274**: 749-751.
- 704 Phillips FM, Zreda MG, Plummer MA *et al.* 2009. Glacial geology and chronology of Bishop Creek and  
705 vicinity, eastern Sierra Nevada, California. *Geological Society of America Bulletin* **121**: 1013-1033.
- 706 Pratt-Sitaula B, Burbank DW, Heimsath AM *et al.* 2011. Topographic control of asynchronous glacier  
707 advances: a case study from Annapurna, Nepal. *Geophysical Research Letters* **38**: L24502.
- 708 Quirk BJ, Moore JR, Laabs BJ *et al.* 2018. Termination II, Last Glacial Maximum, and Late glacial  
709 chronologies and paleoclimate from Big Cottonwood Canyon, Wasatch Mountains, Utah. *Geological  
710 Society of America Bulletin* **130**: 1889-1902.
- 711 Rasmussen S O, Andersen KK, Svensson AM *et al.* 2006. A new Greenland ice core chronology for the  
712 last glacial termination. *Journal of Geophysical Research: Atmospheres* **111**: D06102.
- 713 Refsnider KA, Brugger KA, Leonard EM *et al.* 2009. Last glacial maximum equilibrium-line altitude  
714 trends and precipitation patterns in the Sangre de Cristo Mountains, southern Colorado, USA. *Boreas*  
715 **38**: 663-678.
- 716 Réveillet M, Vincent C, Six D, Rabatel A. 2017. Which empirical model is best suited to simulate glacier  
717 mass balances? *Journal of Glaciology* **63**: 39-54.
- 718 Schildgen T, Dethier DP, Bierman P *et al.* 2002. <sup>26</sup>Al and <sup>10</sup>Be dating of late Pleistocene and Holocene fill  
719 terraces: a record of fluvial deposition and incision, Colorado Front Range. *Earth Surface Processes  
720 and Landforms* **27**: 773-787.
- 721 Schweinsberg AD, Briner, JP, Shroba, RR *et al.* 2016. Pinedale glacial history of the upper Arkansas  
722 River valley: new moraine chronologies, modeling results, and geologic mapping. In Keller SM,  
723 Morgan ML (eds.) *Unfolding the Geology of the West: Geological Society of America Field Guide*,  
724 44; 335-353.
- 725 Small EE, Anderson RS, Repka JL *et al.* 1997. Erosion rates of alpine bedrock summit surfaces deduced  
726 from in situ <sup>10</sup>Be and <sup>26</sup>Al. *Earth and Planetary Science Letters* **150**: 413-425.
- 727 Thackray GD, Lundeen KA, Borgert JA. 2004. Latest Pleistocene alpine glacier advances in the Sawtooth  
728 Mountains, Idaho, USA: reflections of midlatitude moisture transport at the close of the last  
729 glaciation. *Geology* **32**: 225-228.
- 730 Thackray, GD 2008. Varied climatic and topographic influences on Late Pleistocene mountain glaciation  
731 in the western United States. *Journal of Quaternary Science* **23**: 671-681.
- 732 Ullman DJ, Carlson AE, LeGrande AN *et al.* 2015. Southern Laurentide ice-sheet retreat synchronous  
733 with rising boreal summer insolation. *Geology* **43**: 23-26.
- 734 Varhola A, Coops NC, Weiler M *et al.* 2010. Forest canopy effects on snow accumulation and ablation:  
735 an integrative review of empirical results. *Journal of Hydrology* **392**: 219-233.

- 736 Vincent C, Six D. 2013. Relative contribution of solar radiation and temperature in enhanced  
737 temperature-index melt models from a case study at Glacier de Saint-Sorlin, France. *Annals of*  
738 *Glaciology* **54**: 11-17.
- 739 Wagner JD, Cole JE, Beck JW *et al.* 2010. Moisture variability in the southwestern United States linked  
740 to abrupt glacial climate change. *Nature Geoscience* **3**: 110-113.
- 741 Ward DW, Anderson RS, Briner JP *et al.* 2009. Numerical modeling of cosmogenic deglaciation records,  
742 Front Range and San Juan mountains, Colorado. *Journal of Geophysical Research–Earth Surface*  
743 **114**: F01026.
- 744 Widmann BL, Kirkham RM, Houck KG *et al.* 2007. Geologic map of the Fairplay West Quadrangle, Park  
745 County, Colorado. Colorado Geological Survey Open File Report 06-7.
- 746 Young NE, Briner JP, Leonard EM *et al.* 2011. Assessing climatic and non-climatic forcing of Pinedale  
747 glaciation and deglaciation in the western U.S. *Geology* **39**: 171-17  
748



749 **FIGURES**

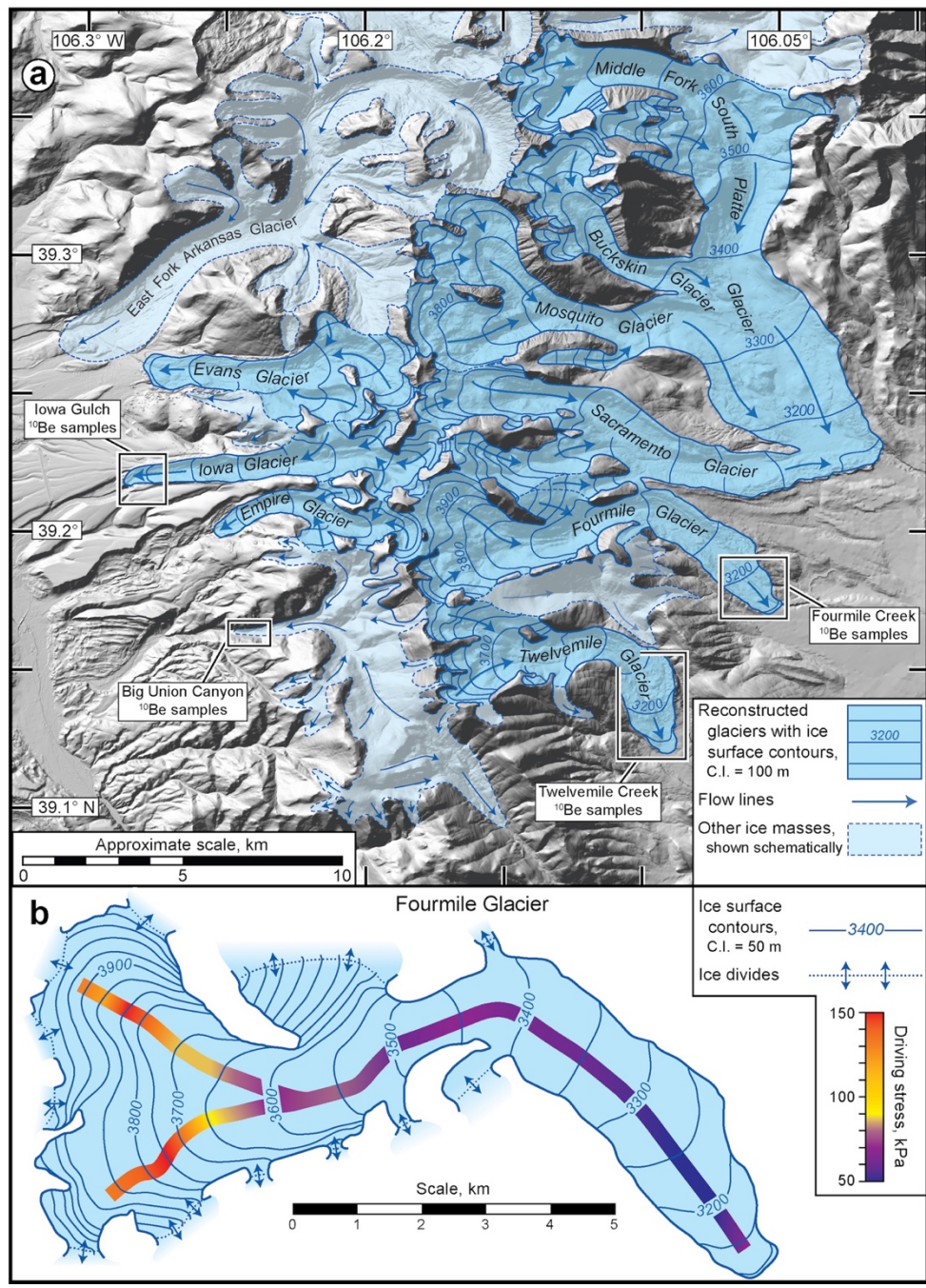
750 **Figure 1.** (a) Location of the study area and surrounding mountain ranges. Area outlined in white is that  
 751 shown in (b). (b) Stations used for modern climate data. Abbreviations: AV Arkansas Valley, BJ  
 752 Buckskin Joe, BV Buena Vista, C Climax, F Fairplay, EM Elks Mountains, FP Fremont Pass, HP Hoosier  
 753 Pass, JH Jones Hill, Leadville (2 stations), MC Michigan Creek, RD Red Deer, RT Rough and Tumble, S  
 754 Salida, SL Sugarloaf Reservoir, SP South Park, SR Sawatch Range, and TL Twin Lakes Reservoir.



755  
 756  
 757  
 758  
 759  
 760  
 761  
 762  
 763  
 764  
 765  
 766  
 767

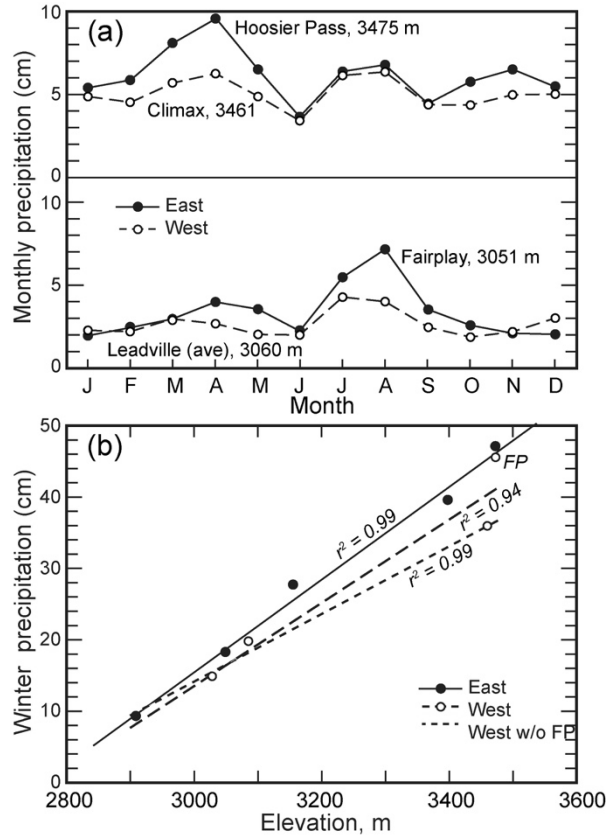


768 **Figure 2.** (a) Reconstructed glaciers of the Mosquito Range during their maximum Pinedale extent. A  
 769 more detailed example is shown in (b). Locations of moraine complexes sampled for surface exposure  
 770 dating are also shown in (a) and correspond to the areas shown in Figure 4.



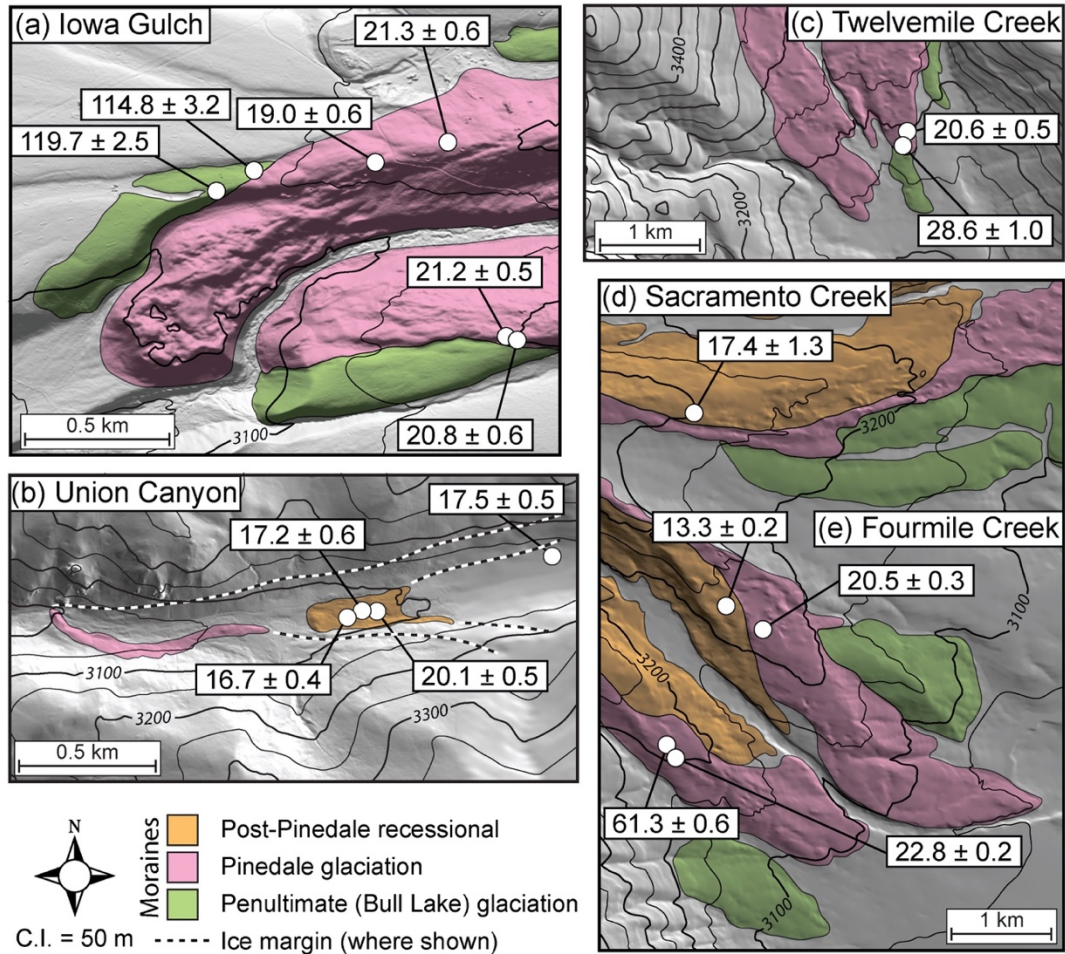
771  
 772  
 773  
 774  
 775  
 776

777 **Figure 3.** (a) Monthly distribution of precipitation at similar high and low elevations on the eastern and  
 778 western slope of the Mosquito Range. Leadville data is a composite of two records. (b) Variation of  
 779 winter precipitation with elevation on the eastern and western slopes of the Mosquito range. Two  
 780 regressions are shown for the western side, one with and one without the Fremont Pass SNOTEL (FP)  
 781 data. See text for discussion.

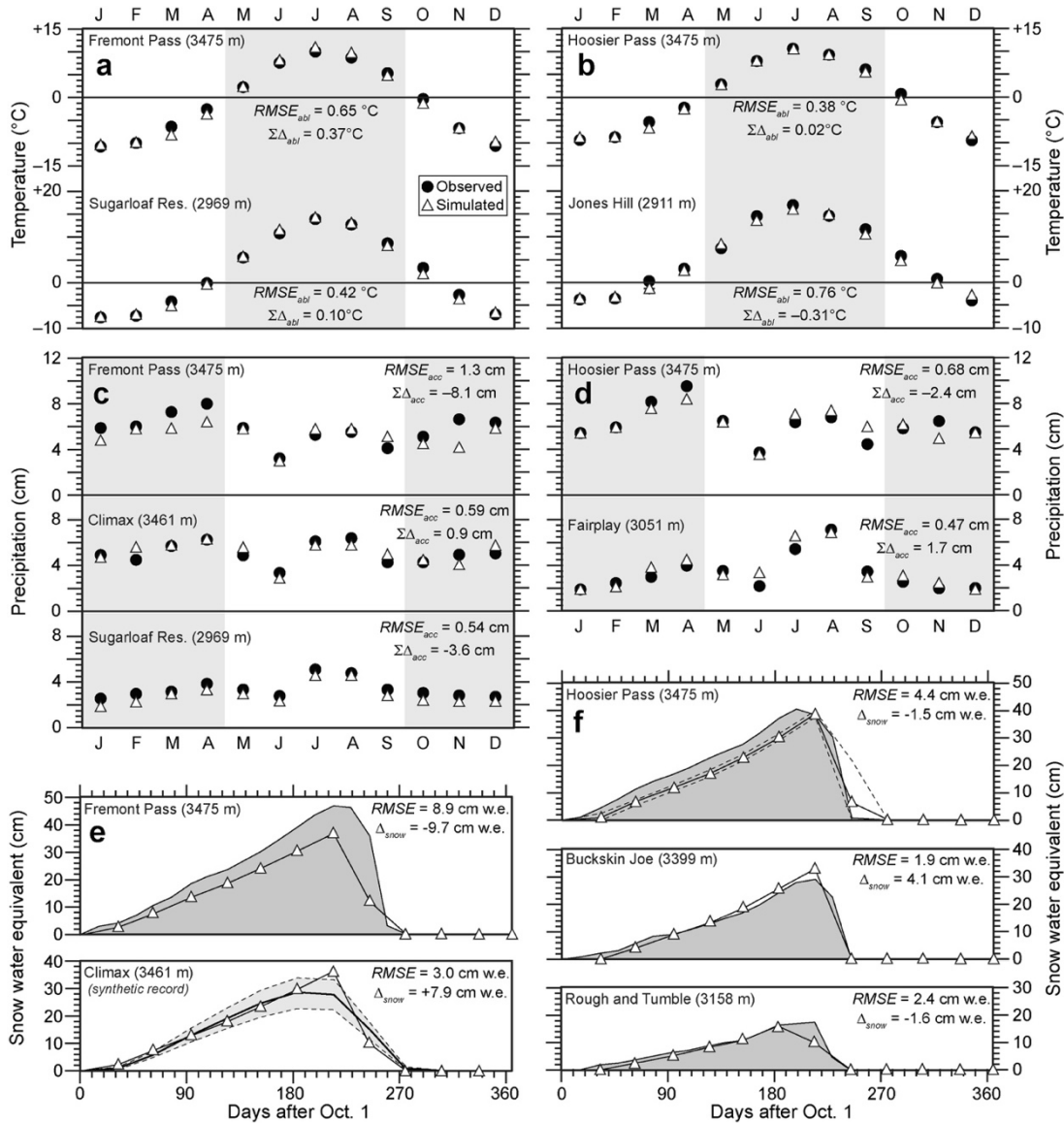


782  
 783  
 784  
 785  
 786  
 787  
 788  
 789  
 790  
 791  
 792  
 793  
 794  
 795  
 796

797 **Figure 4.** Locations of moraine boulders sampled for cosmogenic exposure dating and  $^{10}\text{Be}$  ages (ka) in  
 798 (a) Iowa Gulch, (b) Union Canyon, (c) Twelvemile Creek, and (d) Sacramento Creek and (e) Fourmile  
 799 Creek. Moraine extents and ice margins are simplified and approximate. As noted in the text, boulders  
 800 appropriate for sampling on several of the moraines were very scarce.



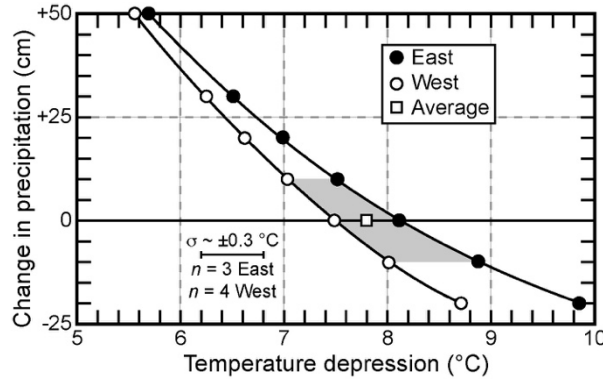
814 **Figure 5.** Comparison of modeled (a and b) monthly temperature, (c and d) monthly precipitation, and (e  
 815 and f) snowpack evolution with observed records at various location in or near the study area. Shaded  
 816 areas in (a-d) highlight the ablation and accumulation seasons respectively. In (e) the shaded area in the  
 817 synthetic record for snowpack evolution at the Climax site shows possible range based on assumed snow  
 818 density. In (f) the uncertainty associated with  $m_f$  values (dashed lines) is only shown for the Hoosier Pass  
 819 site. See text for discussion.



820  
 821  
 822  
 823  
 824  
 825  
 826  
 827



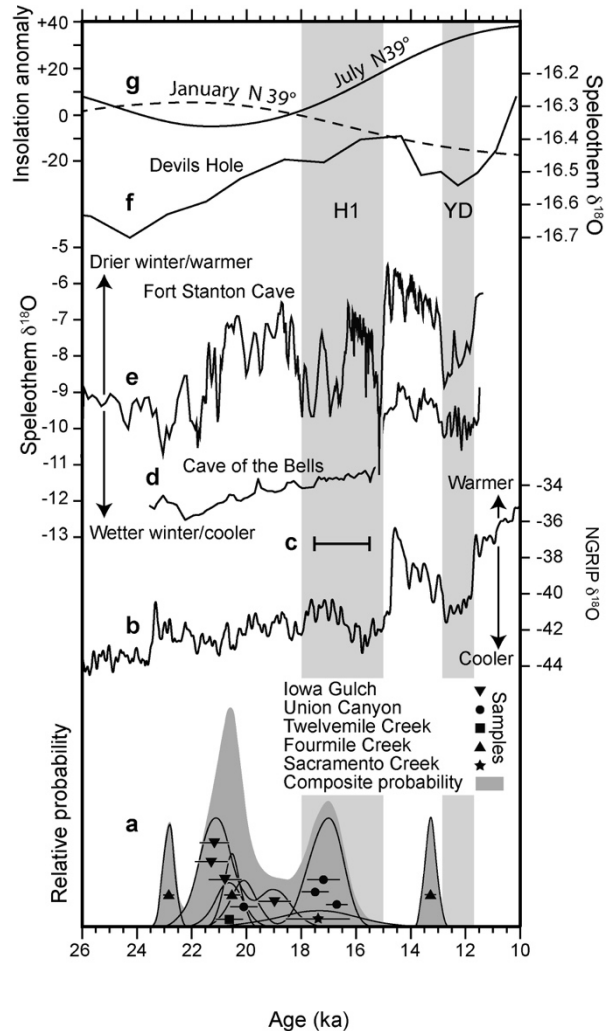
828 **Figure 6.** Combinations of temperature depression and changes in precipitation required to maintain  
 829 steady-state mass balances of paleoglaciers at their maximum Pinedale extents. Mean values for glaciers  
 830 on on eastern and western slopes are shown; standard deviation for each is  $\pm 0.3$  °C. The shaded area  
 831 represents the more likely conditions in the region of the study area based on climate reconstructions. See  
 832 text for discussion.



833  
 834  
 835  
 836

837 **Figure 7.** (a) Probability density plots of  $^{10}\text{Be}$  ages  
 838 for individual moraines and composite for all  
 839 samples shown. Uncertainties shown reflect  $1\sigma$   
 840 internal uncertainty. (b) North Greenland Ice  
 841 Project ice core record of  $\delta^{18}\text{O}$  variations with  
 842 GICC05 chronology (LOESS smoothed;  
 843 Rasmussen et. al, 2006). (c) Timing of the  
 844 dominant highstand of pluvial lakes in the Great  
 845 Basin (Munroe and Laabs, 2013).  $\delta^{18}\text{O}$  variation  
 846 from (d) Cave of the Bells, AZ (Wagner et al.,  
 847 2010), (e) Fort Stanton Cave, NM (Asmerom et al.,  
 848 2010), and (f) Devils Hole, NV (Moseley et al.,  
 849 2016). (g) January and July insolation anomaly at  
 850 39° N (Berger, 1992). Vertical gray bars are the  
 851 Heinrich Stadial (H1; taken here as ~18-15 ka)  
 852 and the Younger Dryas (YD) event.

853  
 854  
 855  
 856  
 857  
 858  
 859  
 860  
 861



862 **Table 1.** Modern climate data\* used in the model and derived values.

863	Station†	Elevation (m)	Mean Temperatures (°C)				Precipitation (cm)				
864			Annual	$T_{jul}$	$T_{jan}$	$H$	Mean annual	Seasonal			
865						$(T_{jul} - T_{jan})$		W	S	S	F
866	<i>East slope</i>										
867	Jones Hill	2911	5.3	16.8	-3.9	20.7	34.3	2.4	7.8	18.8	6.2
868	Fairplay	3051					39.8	6.4	10.4	14.8	8.1
869	Rough and Tumble‡	3158	2.9	12.9	-6.3	19.2	51.6	8.4	16.8	16.0	10.4
870	Michigan Creek	3230	1.9	12.1	-6.4	18.5					
871	Buckskin Joe‡	3399					70.4	15.2	18.9	20.1	16.2
872	Hoosier Pass‡	3475	0.3	10.3	-9.4	19.7	74.7	16.8	24.2	16.9	16.8
873	<i>Mean value</i>					19.5					
874			$dT_{jan}/dz$ (°C m <sup>-1</sup> ) =		-0.0098	$dP_{mod}/dz$ (cm m <sup>-1</sup> ) = 0.026 0.027 0.003 0.020					
875			$r^2$ =		0.95	0.99 0.93 0.13 0.99					
876	<i>West slope</i>										
877	Salida‡	2182	7.4	19.2	-3.1	22.3					
878	Buena Vista‡	2422	6.9	18.7	-3.4	22.1					
879	Red Deer	2682	5.7	16.8	-3.6	20.4	26.6	1.3	8.0	11.1	6.2
880	Twin Lakes‡	2804	3.1	14.7	-7.3	22.0	25.2	3.2	5.7	10.5	5.8
881	Sugarloaf Reservoir‡	2969	2.2	13.7	-7.6	21.3	41.7	8.4	10.5	13.5	9.4
882	Leadville 2SW	3031	1.6	12.7	-8.4	21.1	29.4	5.5	6.7	11.0	6.2
883	Leadville	3088	1.7	13.3	-8.3	21.6	33.7	9.3	8.3	9.4	6.6
884	Climax‡	3461	-0.8	11.1	-10.2	21.3	60.9	14.4	16.9	15.9	13.7
885	Fremont Pass‡	3475	-1.2	10.0	-11.0	21.0	69.3	18.3	21.2	14.0	15.8
886	<i>Mean value</i>					21.5					
887			$dT_{jan}/dz$ (°C m <sup>-1</sup> ) =		-0.0065	$dP_{mod}/dz$ (cm m <sup>-1</sup> ) = 0.019 0.017 0.005 0.012					
888			$r^2$ =		0.91	0.95 0.81 0.60 0.84					

889 \* Different subsets of data were excluded from derivations of lapse rates  $dT_{jan}/dz$  and vertical precipitation gradients  
890  $dP_{mod}/dz$  owing to (1) lack of data, (2) being extreme outliers and/or poor quality, or (3) inappropriate geographic  
891 location or elevation. Precipitation data is less inclusive under the assumption that precipitation is more variable  
892 over the region for than is temperature for given elevation.

893 †Location and station type shown in Fig. 1.

894 ‡1981-2010 climate norm.

895 **Table 2.** Summary of geometric parameters associated with the reconstructed glaciers.

896	Glacier	Area	Length*	Average	Maximum
897		(km <sup>2</sup> )	(km)	thickness†	thickness†
898				(m)	(m)
899	<i>East slope</i>				
900	Twelvemile	20.6	8.0	90	130
901	Fourmile	29.1	13.9	135	170
902	Sacramento	33.5	14.4	135	205
903	South Platte (glacier complex:	113.5	23.3	210	300
904	Mosquito, Buckskin,				
905	and Middle Fork of the				
906	South Platte glaciers)				
907	<i>West slope</i>				
908	Empire	9.2	7.8	100	140
909	Iowa	14.7	11.0	130	175
910	Evans	18.1	9.4	115	155

911 \*Longest flowline

912 †Nearest 5 m

913

914 **Table 3.** Cosmogenic <sup>10</sup>Be exposure ages of moraines (see Supporting Information for details).

915	Valley/Sample ID	<sup>10</sup> Be exposure age (ka)	Internal uncert. (ka)	External uncert. (ka)
916	<i>Union Canyon</i>			
917	UC-03-16	16.7	0.4	0.8
918	UC-04-16	17.2	0.6	0.9
919	UC-01-16	17.5	0.5	0.8
920	UC-02-16	20.1	0.5	0.9
921	<i>Twelvemile Creek</i>			
922	TMC-01-16	20.6	0.5	1.0
923	TMC-02-16	28.6	1.0	1.5
924	<i>Iowa Gulch</i>			
925	<i>Pinedale terminal</i>			
926	IG-04-16	19.0	0.6	1.0
927	IG-05-16	20.8	0.6	1.0
928	IG-06-16	21.2	0.5	0.9
929	IG-03-16	21.3	0.6	1.0
930	<i>Bull Lake terminal<sup>1</sup></i>			
931	IG-02-16	133.2	3.2	6.6
932	IG-01-16	126.9	4.0	6.8
933	<i>Fourmile Creek</i>			
934	FMC-1-2015	13.3	0.2	0.5
935	FMC-2-2015	20.5	0.3	0.8
936	FMC-3-2015	61.3	0.6	2.4
937	FMC-4-2015	22.8	0.2	0.9
938	<i>Sacramento Creek</i>			
939	SC-1-16	17.4	1.3	1.4

940 <sup>1</sup>Assumed erosion rate of 1 mm/kyr.

941 **Table 4.** Inferred LGM temperature depression based on temperature-index simulations.

942 943	Paleoglacier	$\Delta T$ (°C)			ELA* (m)	
		$F = -10$ cm	$F = 0$ cm	$F = +10$ cm	Steady-state	AAR-derived
944	<i>East slope</i>					
945	Twelvemile	-9.3	-8.5	-7.9	3445	3420
946	Fourmile	-8.7	-7.9	-7.3	3505	3480
947	Sacramento	-8.6	-7.9	-7.3	3510	3500
948	South Platte	-8.9	-8.2	-7.6	3480	3435
949	Means $\pm$ standard deviation	$-8.9 \pm 0.3$	$-8.1 \pm 0.3$	$-7.5 \pm 0.3$	$3485 \pm 25$	$3460 \pm 40$
950	<i>West slope</i>					
951	Empire	-7.9	-7.4	-6.9	3590	3555
952	Iowa	-7.9	-7.4	-6.9	3590	3560
953	Evans	-8.2	-7.7	-7.3	3545	3520
954	Means $\pm$ standard deviation	$-8.0 \pm 0.2$	$-7.5 \pm 0.2$	$-7.0 \pm 0.2$	$3575 \pm 25$	$3545 \pm 20$

955 \*For  $F = 1.0$  only; nearest 5 m.

956

957

958 **Table 5.** Regional estimates of LGM temperature depression.

959 960	Location*	Temperature depression, °C**	Methodology†	Reference
961	Mosquito Range	7.5 - 8.2	TI	<i>This study</i>
962	Northern Sawatch Range	6.2 - 7.5	TI	Brugger <i>et al.</i> , 2017; in prep
963	Sawatch Range/Elk Mountains	$6.9 \pm 0.6$	TI	Brugger, 2010
964	Sawatch Range/Elk Mountains	7.0 - 9.0	ELA	Brugger and Goldstein, 1999
965	Sangre de Cristo Mountains	5.0 +1.5/-1.0	EBFM	Leonard <i>et al.</i> , 2017a
966	Sangre de Cristo Mountains	6.0 - 7.5	ELA	Refsnider <i>et al.</i> , 2009
967	Sangre de Cristo Mountains	7.0 - 8.0	TI	Brugger <i>et al.</i> , 2009
968	Front Range	4.5 - 5.8	FM	Dühnforth and Anderson, 2011
969	Colorado Rocky Mountain region	$7.6 \pm 0.7$	ELA	Leonard, 2007
970	Colorado Rocky Mountain region	8.5	ELA	Leonard, 1989

971 \*Locations shown in Figure 1.

972 \*\*Assuming no change in precipitation.

973 †TI = temperature-index model; ELA = climatic interpretation at glacier ELAs; EBFM = coupled energy-balance  
974 and glacier flow model; FM = flow model